applied sciences

MDPI

Article

A Combined Method for Preparation of Landslide Susceptibility Map in Izmir (Türkiye)

Cem KINCAL [1,*] and Hakan KAYHAN [2]

[1] Geological Engineering Department, Engineering Faculty, Dokuz Eylul University, Buca 35390, Izmir, Turkey
[2] The Graduate School of Natural and Applied Sciences, Dokuz Eylul University, Buca 35390, Izmir, Turkey
* Correspondence: cem.kincal@deu.edu.tr or cemkincal@gmail.com; Tel.: +90-23-2301-7344

Abstract: Landslide susceptibility maps (LSMs) have been used frequently by researchers for many years in prediction of the occurrence of landslides. Since many landslides have occurred there in the past, Izmir, which is the third largest city of Türkiye, was selected for landslide susceptibility assessment using geographical information systems (GIS) and remote sensing (RS) techniques. The aim of this study is to create a better landslide susceptibility map (LSM) for the Izmir metropolitan area and its surroundings by minimizing the shortcomings of some of the commonly used methods. For this purpose, four different LSMs were prepared using the logistic regression (LR), analytical hierarchy process (AHP), frequency ratio (FR) and index of entropy (IOE) methods with susceptibility classes ranging from extremely low to extremely high. These four maps were then overlaid. The highest susceptibility class was chosen for each pixel to form a combined landslide susceptibility map (CLSM). The final CLSM is a thematic map presenting landslide susceptibility using five different classes. The geo-environmental factors selected for use in this analysis were slope angle, slope aspect, lithology, slope curvature, elevation, density of discontinuity, stream power index (SPI), land use and distance from stream. Finally, the areas under receiver-operating characteristic (ROC) curves were employed to compare the predictive capability of the five models used. Overall, the Combined Method (CM) (AUC = 0.887) performed very well for landslide susceptibility assessment. Out of all the models, the IOE model (AUC = 0.841) had a slightly lower predictive capability than the CM model, and AHP (AUC = 0.816) was better than FR (AUC = 0.738) and LR (AUC = 0.727). It was observed that, compared to rural areas, residential areas of Izmir city are particularly susceptible to landslides.

Keywords: landslide susceptibility; combined method; analytical hierarchy process; logistic regression; frequency ratio; index of entropy; Izmir (Türkiye)

check for updates

Citation: KINCAL, C.; KAYHAN, H. A Combined Method for Preparation of Landslide Susceptibility Map in Izmir (Türkiye). *Appl. Sci.* **2022**, *12*, 9029. https://doi.org/10.3390/app12189029

Academic Editor: Salvador García-Ayllón Veintimilla

Received: 17 July 2022
Accepted: 3 September 2022
Published: 8 September 2022

1. Introduction

Landslide is described as downslope activity of geological material or mass. Within a soil mass, when gravitational forces or shear stress are greater than shear strength, landslide occurs [1]. The natural factors affecting landslide occurrence are geologic, morphologic and geo-environmental factors. High slope angle values [2], discontinuities [2,3], earthquakes [4,5], heavy rain [2], manmade excavations [6,7] and construction works may also cause stable slopes to fail via zones of weakness [7].

Awareness of these factors, as well their level of influence in triggering landslides makes it easier to foresee future landslides. The best way to assess all the aforementioned geo-environmental factors is to prepare landslide susceptibility maps LSMs. LSMs are viable tools for the analysis of landslides in a particular area and the factors (slope, lithology, aspect, etc.) causing these landslides. The weighting of various the geo-environmental factors must be determined in order to prepare LSMs. One of the main advantages of these maps is the opportunity to work in small scales. Field work in all parts of a large study area would be difficult, expensive and time consuming. After preparing LSMs and determining

which parts of the site are landslide susceptible; field work studies can be concentrated on these sites. Finally, the budget of the project will be affected positively, not only financially, but also in terms of time taken.

Application of different models to different zones is plausible, since landslides in different parts of the world are likely to be affected by different factors. Also, since the behaviour and nature of landslides differ, geo-environmental factors selected in different methods may not correctly simulate the influencing mechanisms. Therefore, it may be necessary to examine applications in different regions, in order to question the performance of these methods.

In the literature, there are many LSMs prepared by various researchers using different methods. In this regard, Çevik and Topal [8] prepared a LSM to find a better location for a natural gas pipeline in Hendek (Türkiye). Authors used the statistical index (Wi) and weighting factor (Wf) methods while preparing LSMs with GIS. They found that Wf was the better method. Lithology was the most important factor in the analyses. Lee [9] used LR and FR analysis in Penang and its surroundings, in Malaysia. The resulting LSM, created using the LR model, showed 7.5% higher accuracy than the FR model. Yalcin et al. [10] used the FR model, AHP, the statistical index (Wi), weighting factor (Wf) and the LR model incorporating GIS and RS techniques to assess landslide susceptibility in Trabzon province (Türkiye). The results were verified using landslide inventory map. According the to results, the Wf method was the best predictive method. Pourghasemi et al. [11] used fuzzy logic and AHP in the surroundings of Alborz folded zone in Iran. Their results showed that the FL model (89.70%) had a better prediction accuracy, at 8.60%, than the AHP model (81.10%). Shahabi et al. [12] used the AHP, FR and LR models on the central Zab basin, Iran. The results revealed that the landslide inventory overlapped for highly and very highly susceptible areas in the AHP (69.41%), FR (73.93%) and LR (75.99%) maps. According to their findings, it was concluded that the LR model gave better results. Pham et al. [13] compared the three techniques—namely, functional trees (FT), multilayer perceptron neural networks (MLP neural nets), and naïve Bayes (NB)—for determining landslide susceptibility in the Uttarakhand region (India). The predictive capability of the factors they used on landslide models was assessed by a linear support vector machine (LSVM) algorithm. The authors concluded that the models they used worked very well for determining landslide-susceptible zones. Abedini and Tulabi [14] used landslide nominal risk factor (LNRF), LR and AHP at the Nojian watershed in Lorestan province, Iran. According to the results, the AHP and LR models showed higher accuracy than the LNRF model. Du et al. [15] used the AHP and LR models in China. The susceptibility map created with FR provided slightly better results than that created with AHP. The researchers stated that the LR method was the best model and could be accepted as the best model for similar situations. Reichenbach et al. [16] reviewed landslide susceptibility studies from 1983 to 2016. The authors emphasized that most recent studies evaluated the model performance and prediction performance, and only a few considered the issue of model uncertainty. They provided suggestions for the generation of landslide susceptibility models with the help of their experience in the field, literature reviews, information analysis using literature database. Talaei [17] prepared a combined model for landslide susceptibility in the northwest of Iran. Landslide hazard potential and resource damage potential layers were combined. Carabella et al. [18] conducted a post-wildfire landslide hazard assessment. The analysis was conducted using a heuristic or expert-based approach with GIS. Finally, they mapped all collected data through an overlay process which could be useful for civil protection warning systems. Demir [19] used the FR and IOE models in Türkiye. As a result, according to the researchers, both methods showed successful results, but the susceptibility map created with the FR yield slightly better results. Konovalov et al. [20] proposed a new probabilistic technique to conduct a risk assessment for landslides triggered by earthquakes. The authors concluded that the approach could improve slope stability studies. Saha et al. [21] used AHP, FR, LR and their ensemble methods in India. According to the results of the study, the AHP model showed 78.86% accuracy, FR model 80.22%,

LR model 80.67%, AHP–FR 83.44%, AHP–LR 84.39% and FR–LR 84.73% accuracy. Sun et al. [22] used logistic regression and the random forest model in China. Although the authors stated that both models provided reasonable results, the random forest model had better stability and predictive capability. Wang et al. [23] used the FR and IOE models in northern Jiangxi Province (China). The researchers concluded that the FR method reached 92.3% accuracy and the IOE method reached 92.3% accuracy, thus both methods had excellent accuracy. Carabella et al. [24] focused on landslides triggered by earthquakes in Central Italy. The authors concluded that the methodology could be used in areas where landslide data are not available. Melese et al. [25] used AHP, FR, and Shannon entropy (SE) in Ethiopia. They found that AHP was the best method compared to the FR and SE models.

The studies above reveal that, benefiting from remote sensing and GIS techniques, various methods can be employed depending on the specifications of the study area and the complexity of the models. These methods can be split into three distinctive categories: statistical methods, multi-criteria decision-making (MCDM), and machine learning (ML). Statistical methods include frequency ratio (Chen et al. [26]; Lee [9]; Lee and Min [27]; Suzen and Doyuran [28]; Lee et al. [29]; Yılmaz [30]; Suzen [31]), index of entropy (Hong et al. [32]; Degirmenci [33]), fuzzy logic (Zadeh [34]), MCDM methods, including AHP (Bathrellos et al. [35]; Rahman et al. [36]; Achour et al. [37]; Sharma et al. [38]; Ali et al. [39]; Akgun ve Turk [40]), ANP methods (Saaty and Vargas [41]), ML methods such as support vector machines (Pradhan [42]; Shirzadi et al. [43]), random forest (Chen et al. [44]; Paudel et al. [45]; Zhang et al. [46]; Kim et al. [47]; Taalab et al. [48]), logistic regression (Iovine et al. [49]; Karimi Sangchini et al. [50]; Polykretis et al. [51]; Lee [9]; Atkinson and Massari [52]; Lee and Min [27]; Dai and Lee [53]; Akgun and Bulut [54]; Akgun [55]; Akgun, et al. [56]; Kıncal et al. [57]), artificial neural networks (Pradhan and Lee [58]; Gorsevski et al. [59]) and so on. MCDM methods are based on expert opinion and experience. Reasonable results can be gathered if the method is applied by a person or group of people who know the study area's conditions well [60]. The parameters related to existing landslides and geo-environmental factors need to be examined properly by means of a detailed field survey in these methods. Expert opinion here may move the analysis forward or may cause some mistakes if it is conducted without experience [40]. Statistical methods are based on the relationship between existing landslide sites and landslide-causing factors. Statistical methods are also used during the analyses. The main advantage of these methods is that the researcher can control weighting values assigned to parameters and final input parameters in statistical assessments [61]. However, the results can be negatively affected if input parameters have multi-collinearity.

The main aim of the machine learning method is to create models which solve potential problems detecting complex systems using old databases [62]. There is no error margin in the algorithmically conducted analyses used in these models. Nevertheless, in this method, the computer not only runs output entered by user but also takes part in decision-making, and the decisions are given without expert opinion, which may produce poor results [63].

Each method has strengths and weaknesses when analyzed and there is no clear winner among the statistical and ML-based techniques. In this study, the combined method (CM) is developed, aiming to combine the strengths of these methods while minimizing erroneous outputs. CM is a viable method to highlight the necessary measures which must be taken for risky situations, to predict unforeseen risky conditions, and to analyze the effects which trigger landslides and enlarge landslide sites. CM is based on combining LSMs with the highest susceptibility prepared using other methods.

Several researchers have utilized a combination of methods in the literature (Do et al. [64]; Fang et al. [65]; Arabameri et al. [66]; Saha et al. [21], etc.). The power of combining methods has also been utilized in novel susceptibility studies such as those examining wildfires (Iban and Sekertekin [67]), floods (Saleh et al. [68]) and gully erosion (Arabameri et al. [69]). The key advantage of this study is that a better LSM was developed helped by the combination of the LR, AHP, FR and IOE methods.

2. Study Area

The study area was Izmir province in Türkiye, located between 38.25° and 38.60° latitude and between 26.90° and 27.35° longitude. Izmir is the third biggest city in west Türkiye (Figure 1a), and has a population of nearly 4.4 million people [70]. The city is very well known, and hosts international cultural activities. Topographically, the altitude reaches 1500 m in the western part of the region. Although a 70° slope can be seen in the working area, the principal slope is between 0° and 35°. Approximately 60% of this zone has a slope gradient <10°. The climate characteristics in the study area are typical Mediterranean climate: seasons are relatively mild, rainy in winter, sunny and hot in summer. Precipitation amounts to 700 mm (27.5 inches) per year, and rain is most abundant in winter; in summer it rains very rarely [71].

Geologically, the rock units can be grouped into three main groups: Bornova mélange, Neogene sediment and Yamanlar volcanic rock. Apart from these three groups, alluvium and slope debris continue to be deposited [72]. The matrix of Bornova mélange rocks located within the tectonic belt called the Izmir–Ankara Zone is composed of Upper Cretaceous–Paleocene sandstone–mudstone intercalations. In the matrix consisting of sandstone–shale intercalations, limestone, serpentinite, chert and diabase blocks of various sizes ranging in age from the Triassic to the Cretaceous can be found [73,74] (Figure 1b).

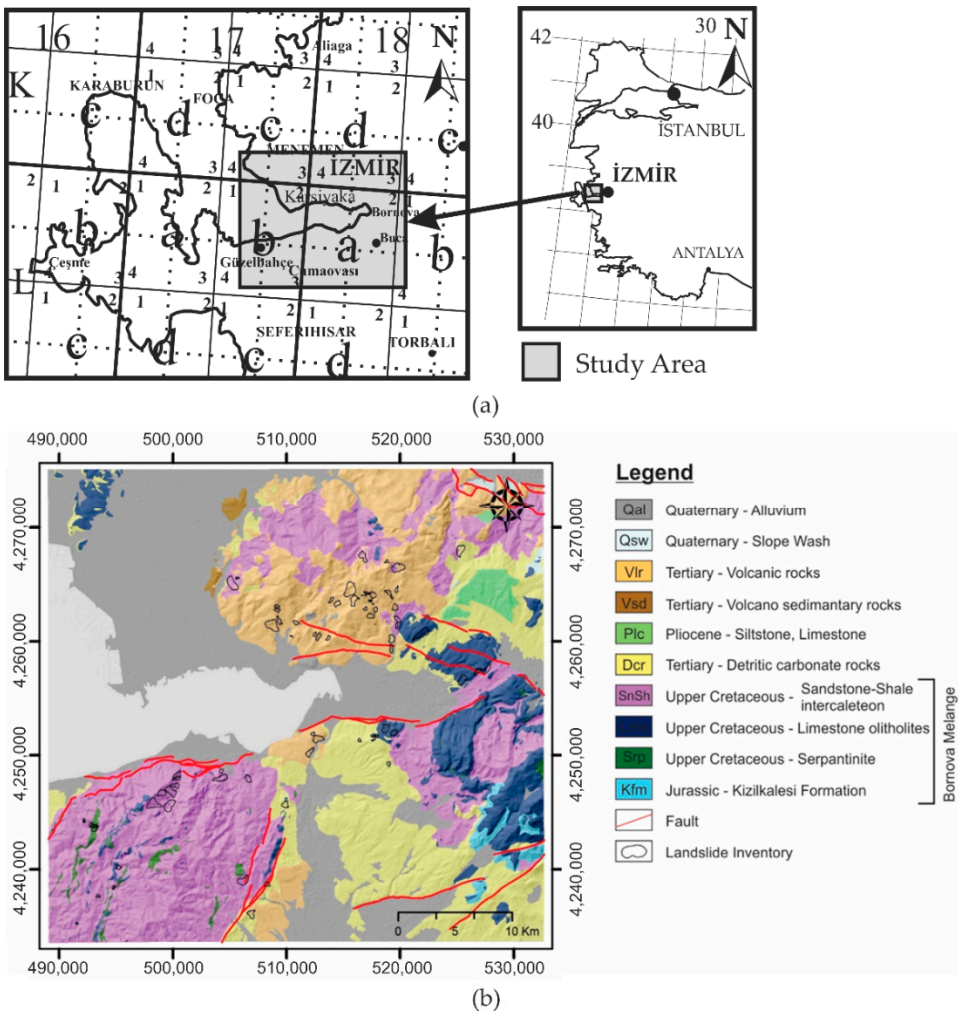

Figure 1. (**a**) Location map, (**b**) Geological map of the study area [75].

Bornova mélange is represented by intercalations of sandstone–shale and the Kizilkalesi formation that occurs in that matrix includes serpentinite blocks and limestone olistoliths (Figure 1b). Lower Miocene–early Pliocene Neogene sedimentary rocks are

angular discordantly overlie the Bornova mélange that forms the bedrock in the study area. The Neogene sedimentary rock deposits are composed of limestone, conglomerate and marl units [76]. The slope angles of the Neogene sedimentary rock layers are close to the horizontal range, between 5–20°. The Upper Miocene and Pliocene Andesitic Yamanlar volcanic rock discordantly overlies the Neogene sedimentary rock [72,77]. The Yamanlar volcanic rock consists of andesite, auto-brecciated andesite, tuff and agglomerates. In the study, the agglomerate and tuff forming the Yamanlar volcanic rock is defined as volcano sediment and the andesite as volcanic rock (Figure 1b).

3. Materials and Methods

This study aims to produce an LSM of the Izmir metropolitan area. First, a landslide inventory map concerning past landslides was created to show the probability of new landslides. Then, the factors that could impair stability (slope angle, slope aspect, lithology, general curvature, elevation, density of discontinuity, stream power index, land use and distance from stream) were selected and those factors were standardized with fuzzy logic [34]. The grid resolution used was 25 × 25 m during the analyses. After standardization, LSMs were produced using together with standardized factors and landslide inventory, using the LR, AHP, FR and IOE methods. In the last stage, the final LSM was produced using the combined method to integrate these four LSMs (Figure 2).

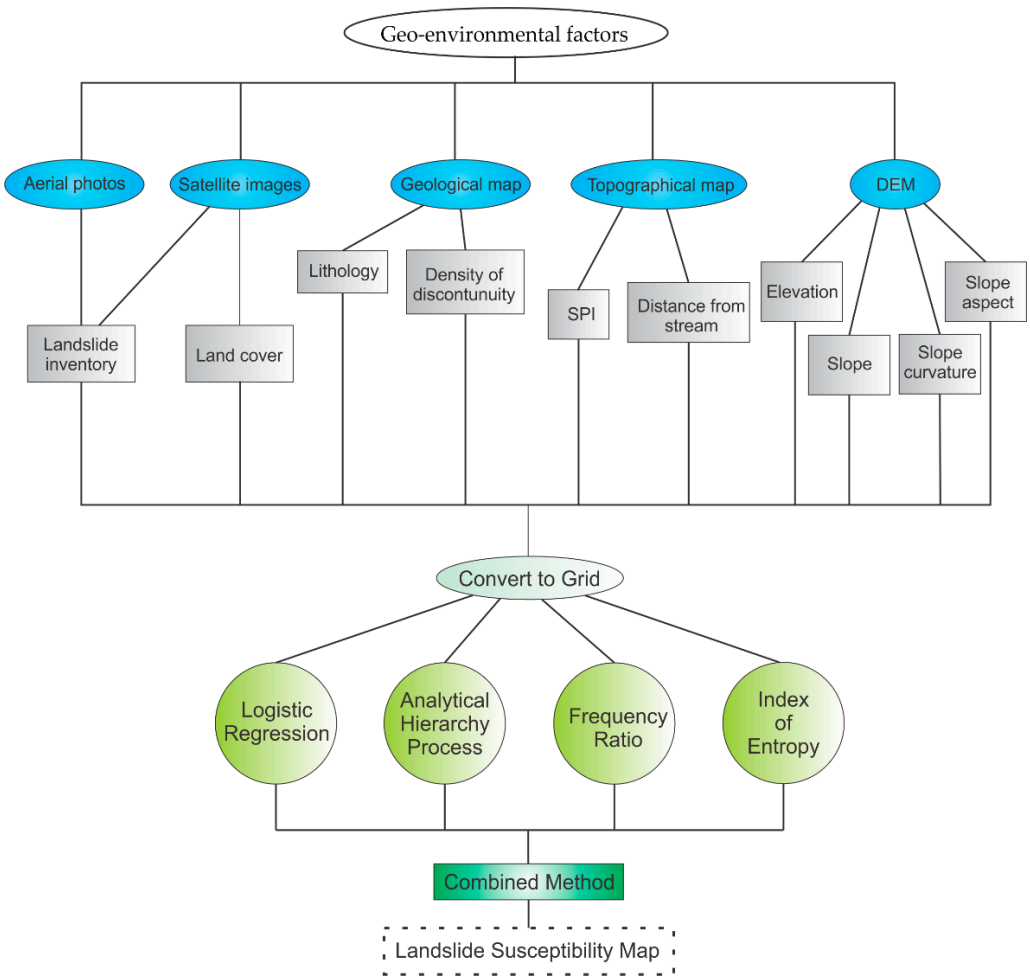

Figure 2. Different steps of combined landslide susceptibility mapping preparation.

3.1. Landslide Inventory

Landslide inventory is the most crucial parameter of landslide susceptibility mapping, since it establishes the connection between landslide formation and the factors causing

this landslide. Chung and Fabbri [78] explain this relationship, noting that "The landslide that occurred due to considered influencing factors will shed light on the formation of new landslides in the future due to the same factors." LSMs can be created by mapping along the borders of the landslide in the field, as well as by remote sensing methods with the help of satellite and aerial photographs [58,79,80]. In this study, the inventory maps created by Avsar [81] and the General Directorate of Mineral Research and Exploration (GDMRE) [82] are combined and enriched with remote sensing data (Figure 3).

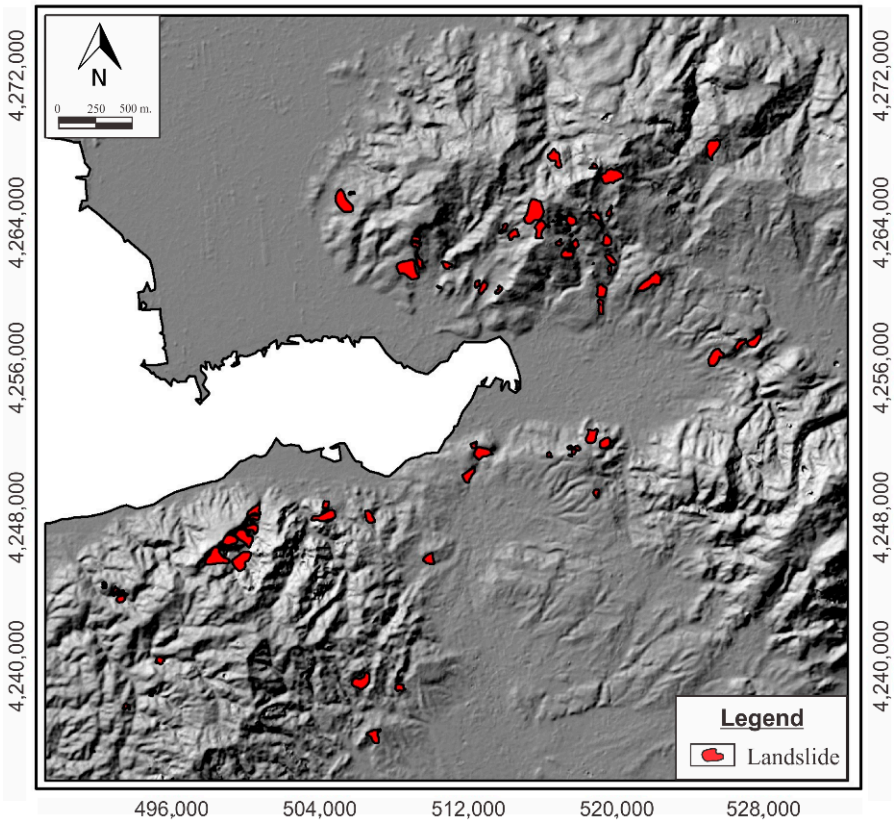

Figure 3. Landslide inventory map of the study area.

3.2. Geo-Environmental Factors: Definition and Statistical Analysis

Conditions that disturb the balance when the rock mass is stable can be defined as geo-environmental factors. Understanding the role of predetermined conditions for landslides is critical to determining the susceptibility of landslide formation [83–85]. For this reason, the correct selection of geo-environmental factors is of great importance in the accuracy of the final LSM being prepared [86]. We can categorize geo-environmental factors into four groups according to their source: geomorphological, geological, hydrological and human. The first three factors relate to causes that are independent of any external effects and occur in completely natural ways. Human factors, on the other hand, are non-natural activities that can disturb stability via the application of surcharge loading on slopes that would otherwise remain stable in nature, for example, via excavation, construction or engineering of the structure in ways that disrupt its stability. In the preparation of the LSM for this study, slope angle, slope aspect, elevation and curvature were taken as geomorphological factors; lithology and density of discontinuity factors as geological factors; stream power index and distance from stream as hydrological factors; and land use as a human factor were used (Table 1). Geo-environmental factors and associated percentages of landslides are given in Figures 4 and 5.

Table 1. Geo-environmental factors used in LSM mapping.

	Group	Data Source	Scale/Resolution	Factor	Data Type
Geo-environmental factors	Geomorphological factors	ASTER GDEM [87]	30*30 m	Slope angle	Numerical
				Slope aspect	Categorical
				Elevation	Numerical
				Slope curvature	Categorical
	Hydrological factors	Topographical map	1/25,000/25*25 m	SPI	Categorical
				Distance from stream	Numerical
	Geological factors	Geological map	1/25,000/25*25 m	Lithology	Categorical
				Density of ciscontinuity	Categorical
	Human factor	Satellite images	30*30 m	Land use	Categorical

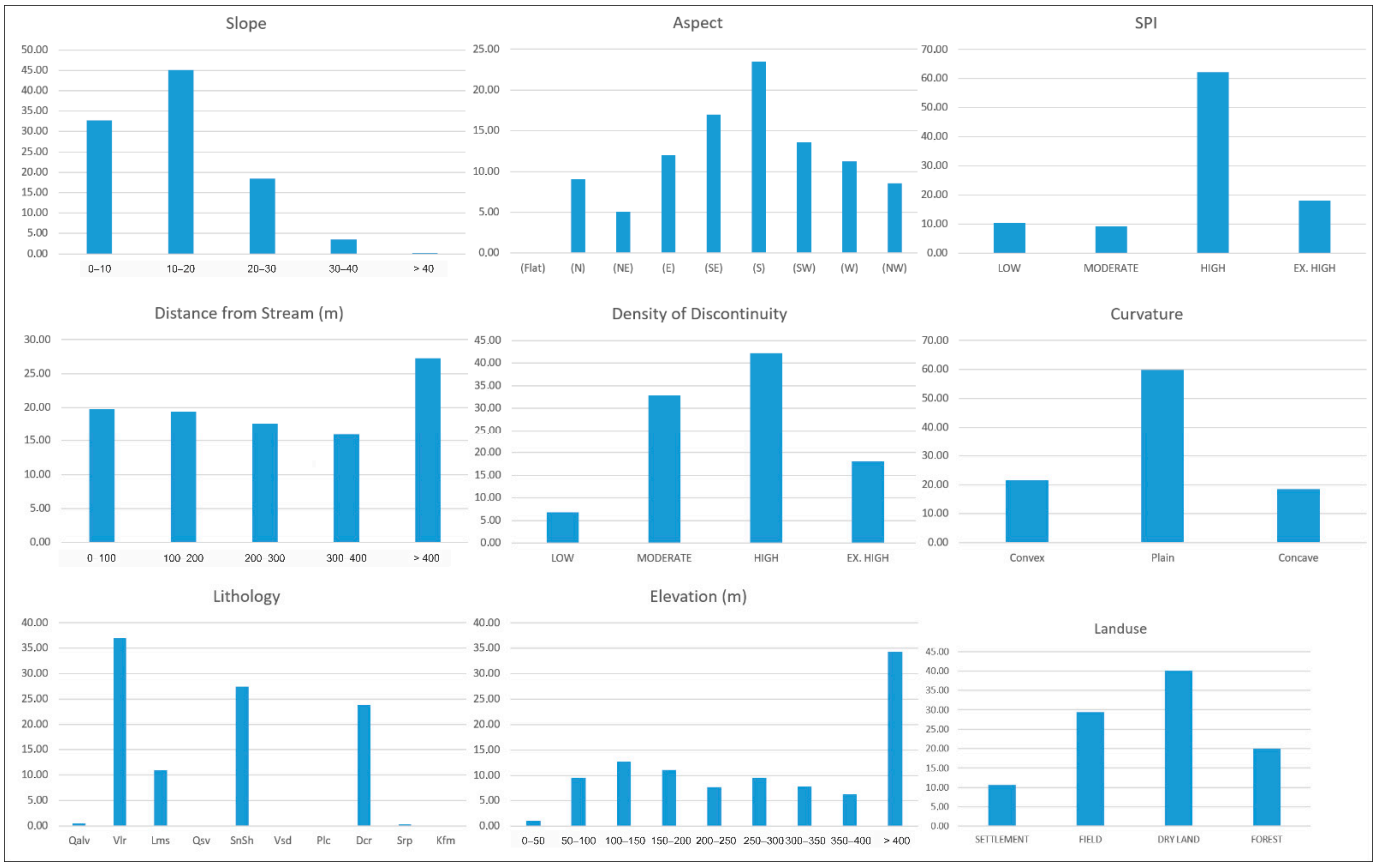

Figure 4. Geo-environmental factors and associated percentages of landslides for evaluation of landslide susceptibility.

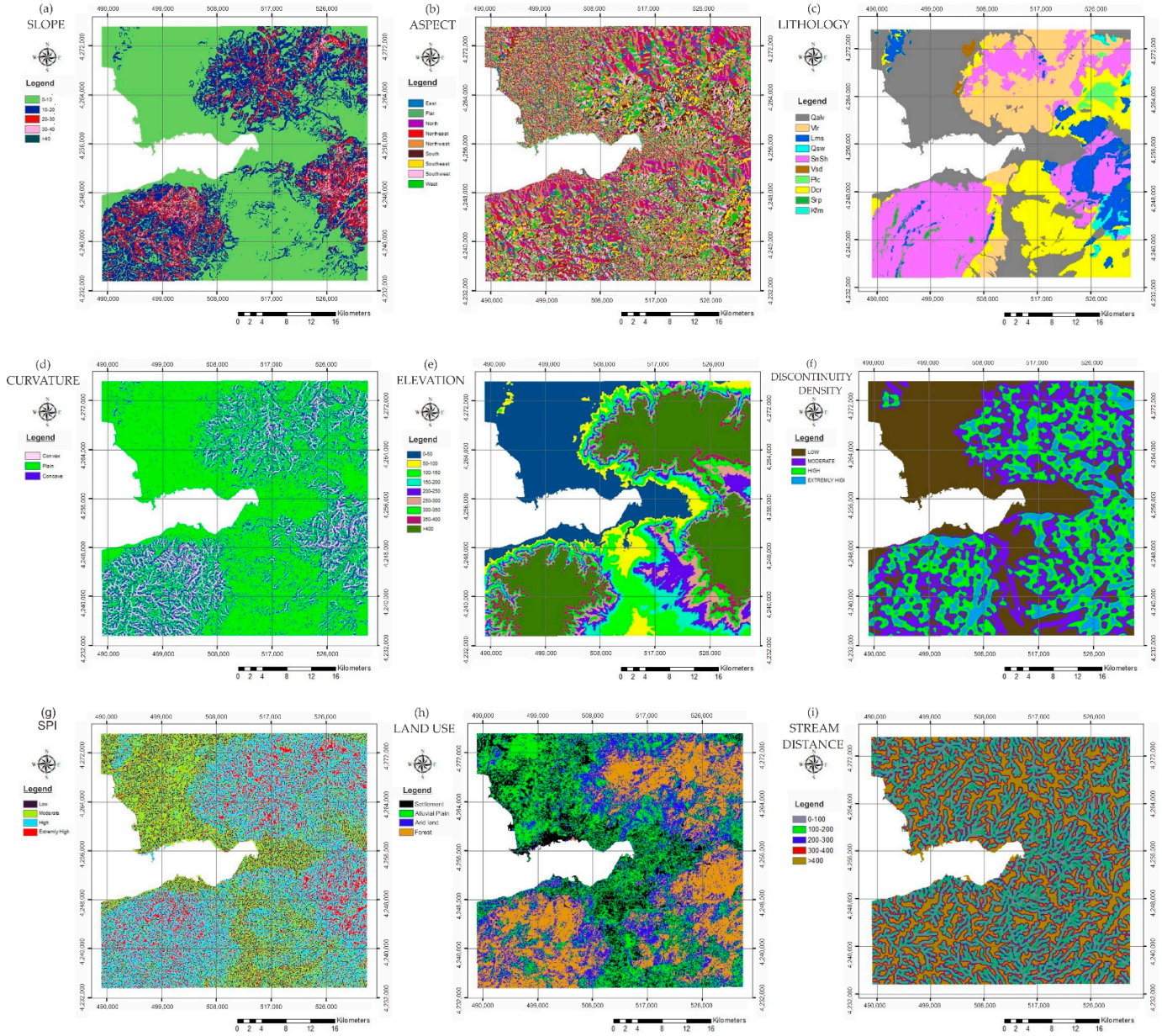

Figure 5. Geo-environmental factors: (**a**) slope, (**b**) slope aspect, (**c**) lithology, (**d**) slope curvature, (**e**) elevation, (**f**) density of discontinuity, (**g**) SPI, (**h**) land use, (**i**) distance from stream.

A 1/25,000 scale geological map of GDMRE, a 1/25,000 scale topographical map, ASTER GDEM data [87], aerial photographs and Google Earth satellite images [88] were used in this study. Lithology and density-of-discontinuity maps were produced from a geological map and ASTER GDEM data [87]. Elevation, slope angle, slope aspect, elevation and slope curvature maps were prepared using ASTER GDEM data (Table 1). SPI and distance-from-stream maps were produced using a topographical map. A land use map was prepared using satellite images. Landslide data from Avşar [81] and GDMRE [82] was used to prepare the landslide inventory map, updated with aerial photographs and Google Earth satellite images [88]. All geo-environmental factor maps were exported to the raster data at 25 × 25 m resolution and the LSMs were produced using this data (Table 1).

Slope angle: This can be defined as the angle made by morphological structures. The slope angle is relevant because the potential for landslide formation increases as the angle increases. This is because as the inclination angle increases, the weight of the rock mass in the direction of the slope increases and eventually the shear stress overcomes the forces

that resist shear and, as a result, mass movement occurs along the surface in the direction of the slope [89].

Slope aspect: The importance of slope direction on landslide formation is still under debate. While some researchers suggest that the slope aspect is an important factor for landslide incidence [90–92], some other researchers think that the slope direction is not that important [52].

Many other parameters such as the groundwater level, the water content of the rock mass and the vegetation growing on the land are causative factors affecting stability. Average precipitation also has a significant effect on these parameters. As it is known that the direction and amount of precipitation in each region may differ according to meteorological conditions, slope aspect in this study is considered an important factor that can affect susceptibility to landslides.

Lithology: This is considered one of the most important factors in LSMs due to its impact on the geo-mechanical properties of a land [93]. Rock type and structural differences usually lead to differences in the strength and permeability of formations [94]. As a result of these differences, the physio-mechanical properties of the rock change. This change will directly affect the shear strength of the rock. On the other hand, the chemical properties and mineralogy of rock affect the rock's resistance to weathering. Rock that loses its physical properties by decomposition will create a higher potential for landslide formation. For this reason, lithology was chosen as the most important geo-environmental factor in preparing the LSMs. The geological map prepared from GDMRE [82] was used for the study area and this map was digitized with ArcMap [95] and converted from "vector" format to raster format to be used in the LSM.

Slope curvature: This is usually obtained by taking the second derivative of a line that occurs at the intersection of the land surface and a plane. A negative value (A) demonstrates that the surface is upwardly convex. A positive profile (B) shows that the surface is upwardly concave. A value of zero means that the surface is linear (C). According to Ohlmacher [96], curvature strongly affects the shear and resistance stresses of landslides, in addition to the water convergence or divergence (drainage) of material in the direction of the landslide's movement. However, researchers do not fully agree on the effect of the curvature parameter on the landslide in the same slope aspect map. Curvature maps are divided into three types: plan curvature maps, profile curvature maps and general curvature maps, a combination of the previous two [89].

Elevation: This is expressed as the height of the slope relative to the sea level; it is one of the parameters commonly used to determine sensitivity to landslides. Altitude may affect vegetation type and precipitation levels [97], therefore elevation directly affects landslide susceptibility. The general trend in landslide susceptibility mapping studies is that areas at higher levels are more sensitive to landslides and as the elevation decreases, the landslide sensitivity decreases.

Density of discontinuity: A discontinuity can be defined as a plane of weakness in rock masses due to bedding with low shear stress, faults, schistosity, etc. When the past landslides are examined, it can be seen that the movement generally follows these planes of weakness, whether at the landslide boundaries or in the slip plane. For this reason, regions where discontinuity planes are concentrated have high potential to create landslides.

Stream power index (SPI): Erosion force is calculated in stream flows using SPI. A stream with a high flow power will erode the surrounding slopes much more along the direction of flow. As a result of the abrasion of the toe, the stability of the slope will deteriorate and the slopes will become more sensitive to landslides. Therefore, landslide susceptibility is much higher in slopes in regions with high stream power index compared to other areas [98]. In this context, the stream power index should be considered an important factor for LSMs.

Land use: This is a geo-environmental factor, categorized based on the evaluation of previous landslides. While factors such as settlement areas, agricultural areas, forest areas, and areas where vegetation is dense or sparse do not cause the formation of landslides

on their own, they are among the factors frequently used in LSMs because resistance to landslide formation will differ under different effects [60].

Distance from stream: As distance to a stream decreases, the increase in groundwater and erosion caused by the bearing power of the stream heightens the probability of landslide formation [99]. Therefore, distance from a stream is a frequently used factor in LSMs.

The slope map was created using ArcMap software's [95] Spatial Analysis Tools and divided into five classes: <10°, 10–20°, 20–30°, 30–40° and >40°. The slope aspect map was created with ArcMap software's Spatial Analysis Tools and divided into nine classes: flat, north, northwest, west, southwest, south, southeast, east and northeast [95]. When preparing the LSM, use of a general curvature map was preferred, since this contains both plan and profile curvature. With the help of ArcMap's [95] Spatial Analysis Tools, a general curvature map was created and divided into three classes: convex, flat and concave. The elevation map was prepared using ArcMap software [95] with the help of a digital elevation model (DEM), and divided into nine classes: >50 m, 50–100 m, 100–150 m, 150–200 m, 200–250 m, 250–300 m, 300–350 m, 350–400 m and >400 m. The discontinuity map was prepared using remote sensing methods, utilizing using aerial photographs of the geology and GDMRE active fault line maps [75]. The density-of-discontinuities map was prepared with the help of ArcMap software [95] and divided into four classes: low, medium, high and very high density. The SPI map was created with ArcMap software's [95] Hydro Tools and divided into four classes: low, moderate, high and extremely high. The land use map produced for this study divided the study area is divided into four classes: forest, arid land, alluvial plain and settlement areas. To prepare the distance from stream map, first a drainage map was prepared and then areas that were 0–100 m, 100–200 m, 200–300 m, 300–400 m and more than 400 m were reclassified according to the distance to these streams.

3.3. Statistical Analysis

3.3.1. Logistic Regression (LR)

Landslide researchers have used various techniques in the production of LSMs due to data and model deficiencies [100]. Multivariate statistical analysis is one of these. LR is one of the most used multivariate statistical analysis techniques. LR allows evaluation of the multivariate regression relationship in landslide susceptibility studies. The advantage of LR is that the variables can be continuous, discrete or any combination of the two [9]. The purpose of LR in this context is to find the most appropriate relationship between the existence of landslides and a set of independent parameters such as slope angle and lithology [101]. For LR studies, the dependent variable should be entered as 0 or 1 so that the model applies correctly to landslide probability analysis. Fuzzy logic can be used to normalize these data between 0 and 1 [40]. The LR algorithm applies maximum probability estimation after converting the dependent variable into a logic variable representing the natural logarithm of the dependent or non-dependent probabilities [92,102]. LR is based on the logistic function given by Equations (1) and (2) [103],

$$P = \frac{1}{1 + e^{-Z}} \tag{1}$$

In this equation, P is assumed to be the estimated value of landslide occurrence varying between 0 and 1, while Z is assumed to be a linear combination of the factors causing the landslide and the factors

$$X_i \text{ (i: 1,2,3, . . . , n)}.Z = B_0 + B_{1 \times 1} + B_{2 \times 2} + \ldots \ldots + B_n X_n \tag{2}$$

where B_0 is the prediction for the intersection and B_1; B_2; . . . .; B_n are estimates for coefficients associated with independent variables. The value Z is found by using the second equation; the value is found after it is replaced in Equation (1) and the landslide probability value (P) is found. In the analysis, Idrisi software [104] geospatial monitoring and modeling system was used to establish the relationship between the area in which landslides occurred

(landslide inventory) and the factors that caused the landslides (slope, slope orientation, lithology, etc.).

The equation for landslide occurrence estimation with LR is given below (Equation (3)).

$$Z = -12.8124 + 5.379812*asp + 0.220848*curve + 0.751963*dod - 0.197740*elv - 0.720106*land + 3.754381*lith + 0.956580*slope + 0.738011*spi - 0.197984*dfs \quad (3)$$

In this equation, "asp" is slope aspect, "curve" is curvature, "dod" is density of discontinuity, "elv" is elevation, "land" is land use, "lith" is lithology, "slope" is slope angle, "spi" is stream power index and "dfs" is distance from stream.

A summary of the basic statistics of the LR model obtained using Idrisi software [97] Logistic reg tools is given in Table 2. Of the values included in these statistics, a pseudo-R^2 equal to 1 indicates perfect fit, while 0 indicates no relevance. The pseudo-R^2 value shows how well the logit model fits the dataset. A pseudo-R^2 greater than 0.2 shows a relatively good fit [105]. In this study, the pseudo-R^2 value was calculated as 0.1607 (Table 2). In addition, a value of 0.8499 was obtained for the relative operating characteristic (ROC), which can be considered a sign of good correlation between the independent and dependent variables.

Table 2. Summary of statistics of the logistic regression model.

Statistics	Value
Total number of pixels	2,908,836
−2logL0	27,433.052
−2log(likelihood)	23,025.032
Pseudo-R^2	0.1607
Goodness of fit	207,434.51
Area under the ROC curve	0.727

3.3.2. Analytical Hierarchy Process (AHP)

The AHP, a multi-criteria decision-making method, involves matrix-based binary comparison of the contribution of various factors, providing a flexible and understandable way to analyze complex problems [106]. AHP is beneficial as it has the ability to handle both qualitative and quantitative criteria [107]. Regardless of data type, use of AHP functions is feasible because the basic input is given by the user. Answers to questions such as "How important is parameter A compared to parameter B?" represent expert decisions. The relative importance of the parameters was converted into a nine-point continuous rating scale. It was then entered into the binary comparison matrix (Table 3).

Table 3. Scales for pairwise comparisons [108].

Importance	Definition	Explanation
1	Equal importance	Contribution to objective is equal
3	Moderate importance	Attribute is slightly favored over another
5	Strong importance	Attribute is strongly favored over another
7	Very strong importance	Attribute is very strongly favored over another
9	Extreme importance	Evidence favoring one attribute is of the highest possible order of affirmation
2, 4, 6, 8	Intermediate values	When compromise is needed
Reciprocals	Opposites	Used for inverse comparison

At the beginning of the analysis, using the importance values in the Table 3, a binary comparison matrix was created between the parameters that cause landslides. However, pairwise comparison is subjective and the quality of results is highly dependent on expert

judgment. The consistency rate is used to control this expert decision. Equation (4) shows how to calculate the consistency ratio [109].

$$\mathrm{CR} = \mathrm{CI}/\mathrm{RI} \tag{4}$$

"RI" is the average of the consistency index that arises depending on the order of the matrix given by Saaty [109]. "CI" in Equation (5) is the consistency index.

$$\mathrm{CI} = (\lambda_{\max} - \mathrm{n})/(\mathrm{n} - 1) \tag{5}$$

Here, "$\lambda_{\max}$" is the largest or fundamental eigenvalue of the matrix and can be easily calculated from the matrix and "n" is the order of the matrix.

3.3.3. Frequency Ratio (FR)

FR is a method frequently used by researchers because the method is based on extremely simple and uncomplicated calculations. The main logic of the method is to associate the parameters that caused a landslide with the landslide inventory and, with the help of these connection, determine other sites susceptible to landslides. To establish this connection, first the percentage of pixels with landslide-occurred terrain (a) and the percentage of pixels landslide-free terrain (b) must be calculated. Then, the FR is calculated for each parameter with the equation "a/b" [110].

3.3.4. Index of Entropy (IOE)

Entropy in thermodynamics represents the thermal energy of a system that cannot be converted to mechanical work. It is often defined as the randomness and disorder (chaos) in a system. Entropy shows the extent of instability, disorder and uncertainty in a system [111]. The entropy level of a system has a one-to-one relevancy with the degree of disorder. This relevancy, called the Boltzmann principle, is used to describe the thermodynamic state of a system [111]. An entropy model for information theory was established using the Boltzmann principle by [112]. The IOE method is widely used to determine the weight index of natural hazards [113–115].

As noted by Ren [116], a "landslide is a complex system for material and energy exchange with the environment and therefore a landslide can be measured and defined using the information entropy method". The entropy of a landslide refers to the degree to which different factors affect the progress of a landslide [117]. Some important factors, such as slope, lithology and curvature, produce additional entropy to the index system. Finally, the level of entropy can be used to determine the objective weights of the index system [117–119]. The following steps are used to compute the weight values of geo-environmental factors and to produce the LSM using these weighted values.

The following equations (Equations (6) and (7)) are used to calculate the information coefficient "W_j", corresponding to the weight value of the parameter as a whole [119–121]:

$$P_{ij} = \frac{a}{b} \tag{6}$$

$$(P_{ij}) = \frac{P_{ij}}{\sum_{j=1}^{S_j} P_{ij}} \tag{7}$$

where "a" and "b" are percentages of landslide-free area and landslide-occurred area, respectively. "S_j" is the number of classes and (P_{ij}) is the probability density. "H_j" and "H_{jmax}", indicated by Equations (8) and (9) below, represent the entropy values.

$$H_j = \sum_{i=1}^{S_j} (P_{ij}) \log_2 (P_{ij}),\ J = 1, 2, \ldots, n \tag{8}$$

$$H_{jmax} = \log_2 S_j \tag{9}$$

"I_j" is the information coefficient calculated by Equation (10) and "W_j", calculated by Equation (11), represents the weight of the parameter as a whole.

$$I_j = \frac{H_{jmax} - H_j}{H_{jmax}} \; I = (0,1), \; J = 1,2,\ldots,n \tag{10}$$

$$W_j = I_j \times P_{ij} \tag{11}$$

3.3.5. Combined Method (CM)

Various methods have been developed in many landslide susceptibility studies, and countless studies have been conducted using these methods. Investigating these studies, it is clear that each method has advantages and disadvantages. The combined method was developed to minimize the errors that these disadvantages might cause. The logic behind the method is that superimposing LSMs created using various methods will result in a susceptibility map with the highest reliability. The combined method procedure involves assigning each pixel the highest landslide susceptibility score among all the data obtained for that pixel from the LSMs prepared using different methods for a specific geographical point (Figure 6). The aim here is to conduct more reliable studies and minimize the risk of errors by choosing the higher susceptibility value as the landslide susceptibility of a certain pixel where method "A" indicates low susceptibility and method "B" indicates high susceptibility. In order to prepare an LSM with the combined method, it is necessary to prepare LSMs based on between two and four methods and overlay these maps. The results obtained indicate that the combined method yields the greatest reliability when the highest number of susceptibility maps prepared with different methods are overlaid. However, using more than four methods is considered not to lead to higher reliability, therefore a maximum of four methods for preparing LSMs should be used and the combined method should be applied with these maps.

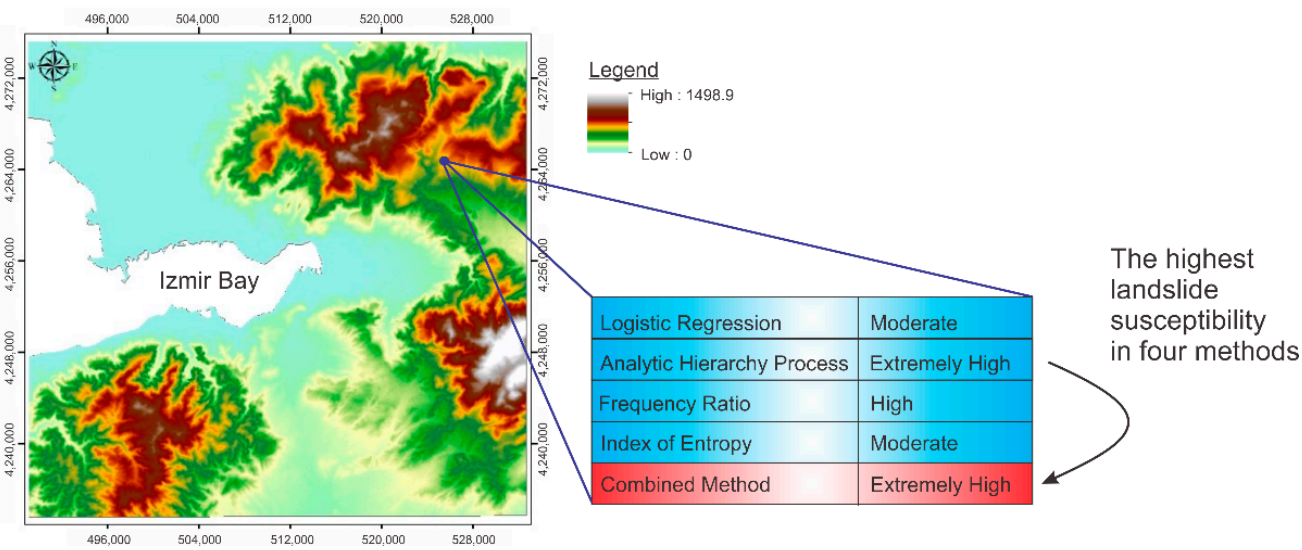

Figure 6. Details of the combined method, highest susceptibility class out of four methods is assigned.

LR, AHP, FR and IOE are the most frequent four methods selected in recent landslide susceptibility mapping studies. Four different LSMs were prepared using these methods and overlaid using ArcGIS Spatial Analyst Tools. Then, all pixels were reclassified in the study area after choosing the pixel value with the highest landslide susceptibility among to the four methods (Figure 6). As a result of this combined method classification process, the final LSM was classified according to five groups, from lowest susceptibility to highest (Figure 6).

4. Results and Discussion

Four LSMs were produced using the LR, AHP, FR and IOE methods for Izmir city and its surroundings. Maps prepared for the geo-environmental factors slope angle, slope aspect, lithology, slope curvature, elevation, density of discontinuities, stream power index, land use and distance from stream used during analyses are given in Figure 5 and their landslide susceptibility properties are given in Figure 4. The natural breaks method was used to generate zoning criteria in the preparation of all four landslide susceptibility maps.

4.1. Comparison of LSM Results

For analysis with LR, in order to determine the probability of landslide occurrence in a certain area, probability was calculated using Equation (1) and the file was converted to raster format to obtain an LSM. The probability of landslide occurrence is given as a value between zero (0) and one (1), and the LR map has a pixel size of 25 × 25 m. The LR-based map classified the data into five groups, from extremely low to extremely high (Figure 7).

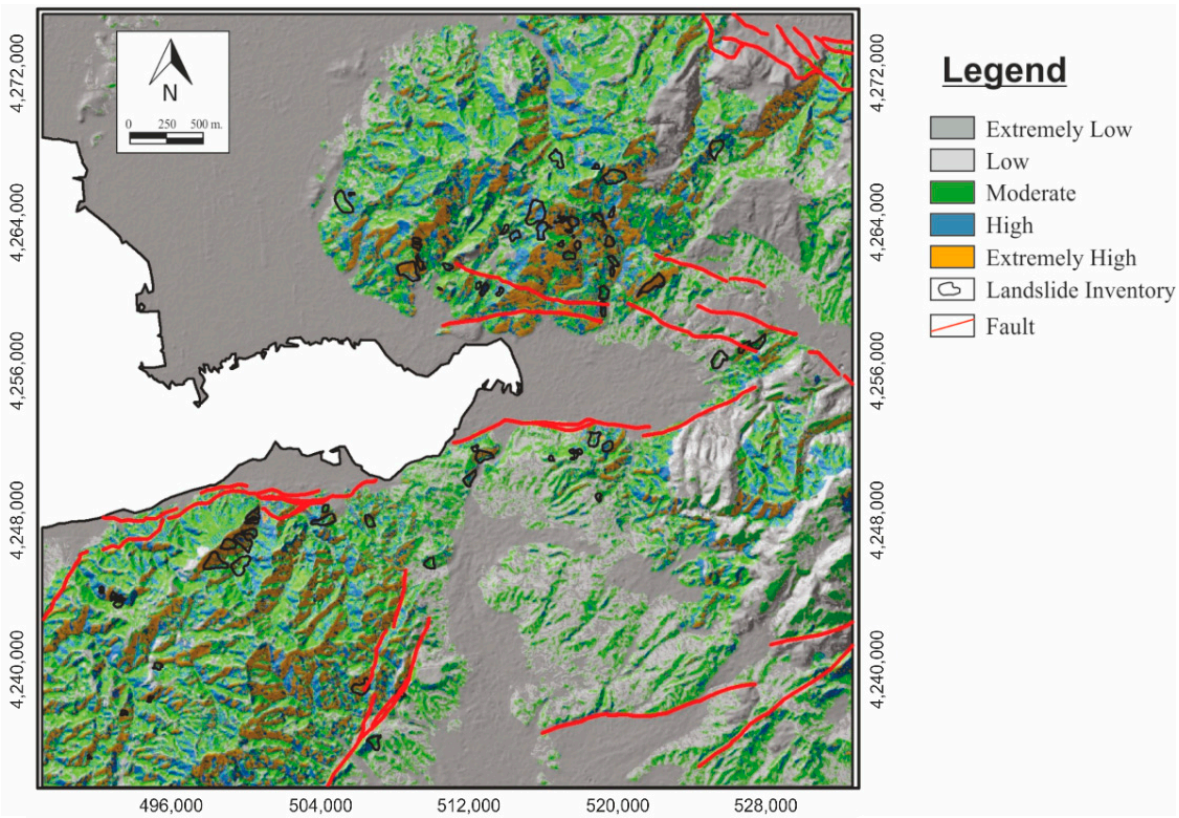

Figure 7. Landslide susceptibility map prepared with LR method.

With the AHP method, if the consistency ratio values are less than 0.1 the binary comparison matrix is acceptable, but if the values are greater than 0.1 then the comparisons must be reassessed [121]. In this study, the consistency rate was 0.03, indicating a reasonable level of consistency in pairwise comparison (Table 4). Paired comparison according to the consistency ratio is good enough to recognize the factor weights in the landslide susceptibility model. The LSM prepared using AHP method is given in Figure 8. The weighting of the parameters in the LSM via matrix was calculated using Idrisi's [104] weighting module and was divided into five classes, from extremely low to extremely high.

Table 4. Pair-wise comparison matrix, factor weights and consistency ratio of the data layers.

Parameter	1	2	3	4	5	6	7	8	9	Weight
(1) Slope aspect	1									0.1617
(2) Density of discontinuity	1/2	1								0.1113
(3) Lithology	1	2	1							0.1617
(4) Slope	2	3	2	1						0.2716
(5) SPI	1/4	1/3	1/4	1/6	1					0.0458
(6) Slope curvature	1/5	1/4	1/5	1/7	1/2	1				0.0307
(7) Elevation	1/6	1/5	1/6	1/8	1/3	1/2	1			0.0221
(8) Land use	1	1	1	1/2	4	5	6	1		0.1495
(9) Distance from stream	1/4	1/3	1/4	1/6	1	2	3	1/4	1	0.0458
Consistency ratio: 0.03										

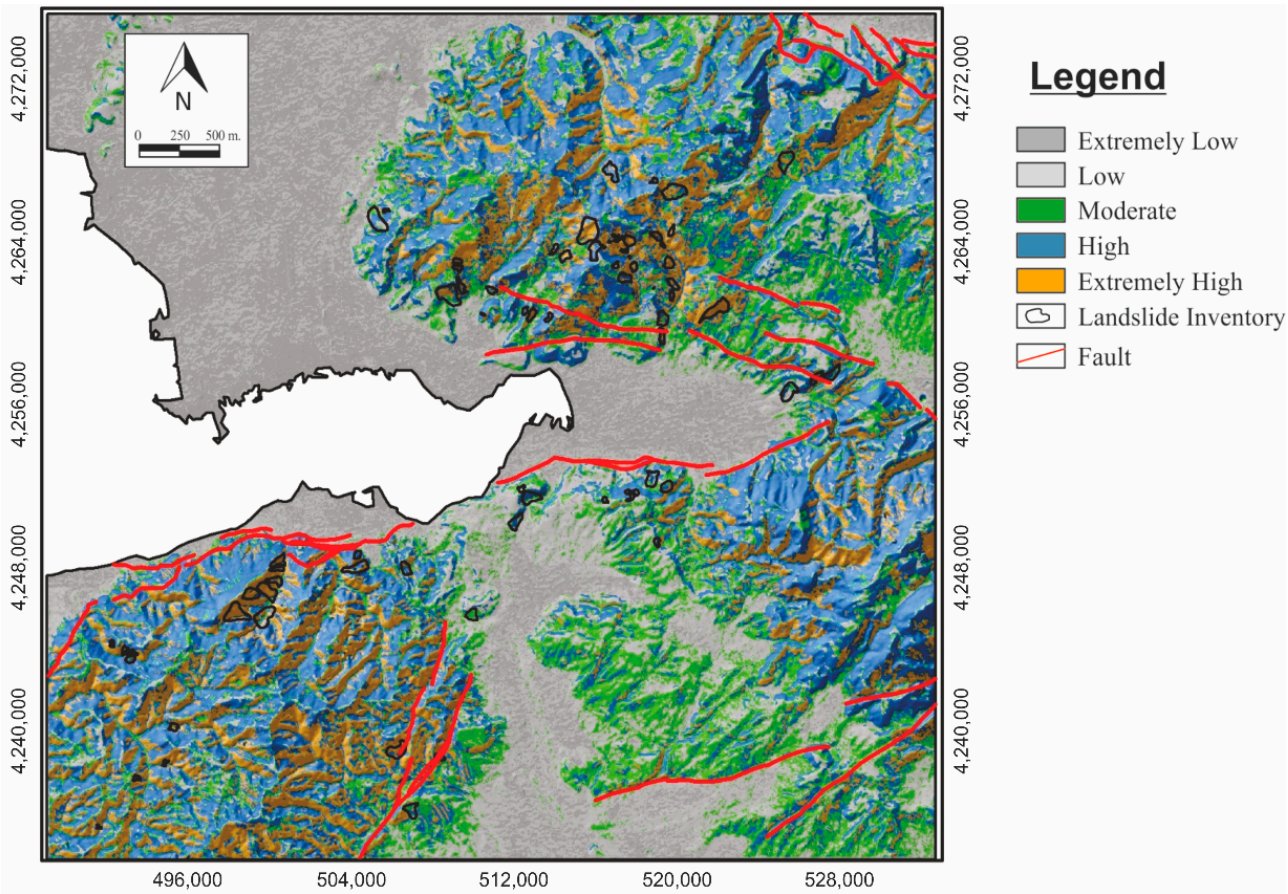

Figure 8. Landslide susceptibility map prepared with AHP method.

In cases where these calculated FR values are less than 1, the effect of this parameter on landslides may be low. In cases where it is greater than 1, the effect of this parameter on landslides can be considered high. FR values for causative factors are given in Table 5. In this study, the LSM based on the FR method was classified using the natural breaks method and divided into five classes, from extremely low to extremely high (Figure 9).

Table 5. FR values for causative factors.

Factor	Class	No. of Pixels in Domain	Percentage of Domain	No. of Landslide	Percentageof Landslide	FR	Normalized Frequency Ratio
Slope (Deg)	0–10	1,527,794	60.43	14,109	32.72	0.54	0.31
	10–20	678,851	26.85	19,454	45.12	1.68	0.95
	20–30	266,839	10.55	7966	18.47	1.75	0.99
	30–40	49,548	1.96	1491	3.46	1.76	1.00
	>40	5163	0.20	100	0.23	1.14	0.65
Aspect	Flat	29,326	1.16	0	0.00	0.00	0.00
	N	312,627	12.37	3910	9.07	0.73	0.42
	NE	259,456	10.26	2174	5.04	0.49	0.28
	E	247,899	9.81	5175	12.00	1.22	0.70
	SE	299,619	11.85	7315	16.96	1.43	0.82
	S	338,804	13.40	10,140	23.52	1.75	1.00
	SW	330,225	13.06	5856	13.58	1.04	0.59
	W	343,688	13.59	4858	11.27	0.83	0.47
	NW	366,551	14.50	3692	8.56	0.59	0.34
SPI	Low	434,163	17.17	4457	10.34	0.60	0.37
	Moderate	667,197	26.39	3997	9.27	0.35	0.21
	High	1,145,730	45.32	26,856	62.28	1.37	0.84
	Ex. high	281,105	11.12	7810	18.11	1.63	1.00
Distance from stream (m)	0–100	628,808	24.87	8536	19.80	0.80	0.62
	100–200	536,113	21.21	8353	19.37	0.91	0.70
	200–300	450,044	17.80	7591	17.60	0.99	0.77
	300–400	377,276	14.92	6863	15.92	1.07	0.83
	>400	535,954	21.20	11,777	27.31	1.29	1.00
Density of discontinuity	Low	803,727	31.79	2925	6.78	0.21	0.11
	Moderate	766,508	30.32	14,,173	32.87	1.08	0.56
	High	720,240	28.49	18236	42.29	1.48	0.77
	Ex. high	237,720	9.40	7786	18.06	1.92	1.00
Curvature	Convex	367,398	14.53	9300	21.57	1.48	1.00
	Plain	1,773,818	70.16	25,822	59.88	0.85	0.57
	Concave	386,979	15.31	7998	18.55	1.21	0.82
Lithology	Qalv	750,212	29.71	213	0.49	0.02	0.00
	Vlr	362,782	14.37	15,952	36.99	2.57	1.00
	Lms	201,654	7.99	4715	10.93	1.37	0.53
	Qsv	7848	0.31	0	0.00	0.00	0.00
	SnSh	688,762	27.28	11,822	27.42	1.00	0.39
	Vsd	9260	0.37	0	0.00	0.00	0.00
	Plc	30,337	1.20	0	0.00	0.00	0.00
	Dcr	429,522	17.01	10,267	23.81	1.40	0.55
	Srp	21,359	0.85	120	0.28	0.33	0.13
	Kfm	22,983	0.91	0	0.00	0.00	0.00
Elevation (m)	0–50	607,148	24.02	458	1.06	0.04	0.03
	50–100	161,965	6.41	4105	9.52	1.49	0.94
	100–150	219,961	8.70	5473	12.69	1.46	0.92
	150–200	175,781	6.95	4764	11.05	1.59	1.00
	200–250	209,613	8.29	3342	7.75	0.93	0.58
	250–300	170,361	6.74	4115	9.54	1.42	0.89
	300–350	154,400	6.11	3352	7.77	1.27	0.80
	350–400	125,978	4.98	2701	6.26	1.26	0.79
	>400	702,988	27.81	14,810	34.35	1.24	0.78
Land use	Settlement	362,269	14.33	4607	10.68	0.75	0.51
	Field	731,306	28.93	12,645	29.33	1.01	0.69
	Dry land	690,159	27.30	17,266	40.04	1.47	1.00
	Forest	742,845	29.38	8602	19.95	0.68	0.46

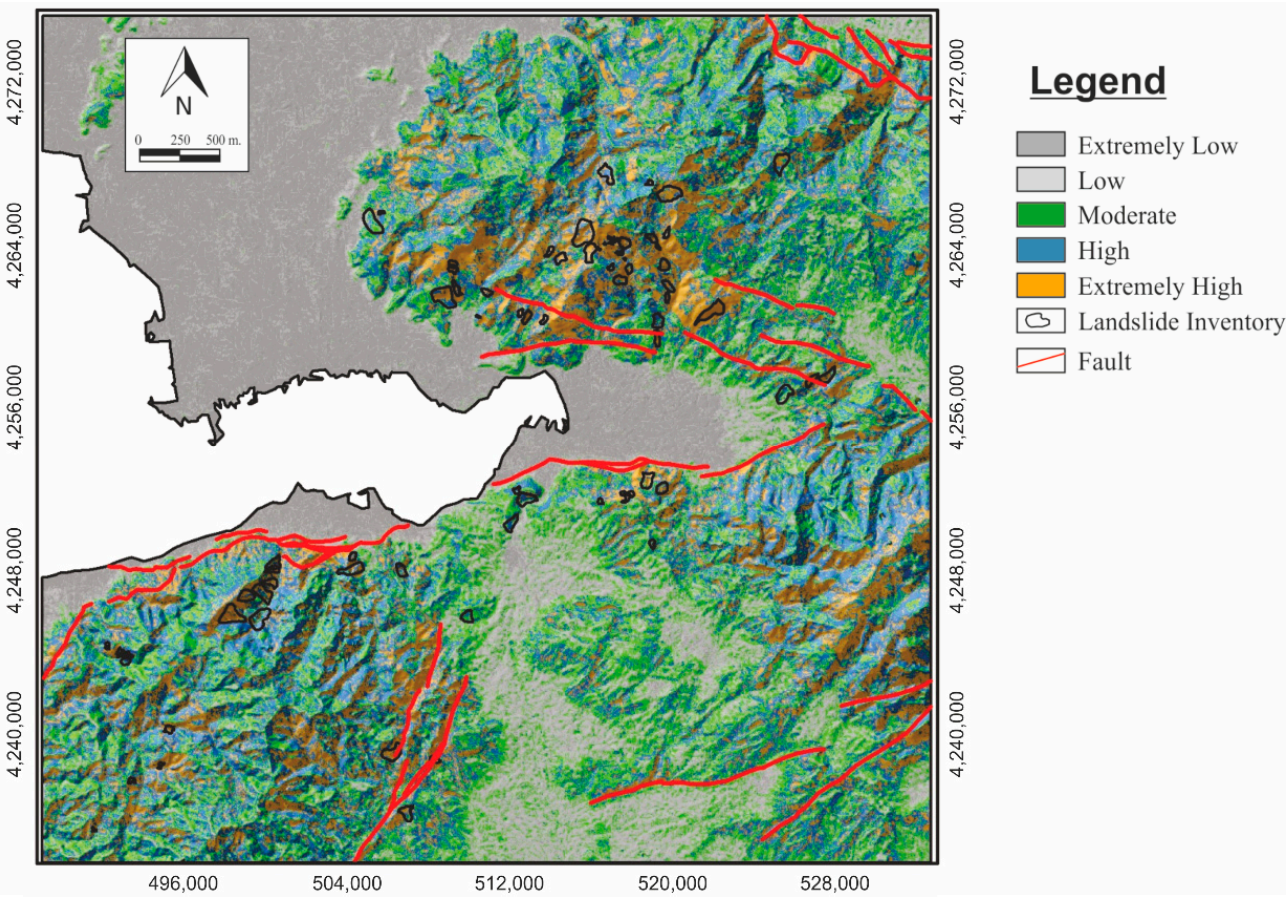

Figure 9. Landslide susceptibility map prepared with the FR method.

The LSM produced by the IOE method was classified using the natural breaks method and divided into five classes, from extremely low to extremely high. IOE values for causative factors are given in Table 6. The LSM prepared with IOE method is given in Figure 10.

In order to finalize the mapping, the abovementioned analysis results were overlaid on a pixel basis, and the LSMs produced by the LR, AHP, FR and IOE methods were combined with the help of ArcMap software's [95] Spatial Analyst Tools. The susceptibility map produced by the combined method was reclassified into five classes, from extremely low to extremely high, using the natural breaks method (Figure 11). A graph showing the percentages of susceptibility classes in the landslide inventory map and susceptibility classes in the study area is given in Figure 12.

It was determined that in the LSM prepared using LR method, the existing landslide areas' susceptibility classes were: 2.07%—extremely low, 8.84%—low, 28.82%—moderate, 25.57%—high and 34.7%—extremely high. The AHP-based LSM showed landslide susceptibilities classes of 0.19%—extremely low, 6.27—ow, 12.01%—moderate, 36.7%—high and 44.84%—extremely high. For the FR method, the values were found to be 0.18%—extremely low, 2.72%—low, 10.93%—moderate, 31.88%—high and 54.29%—extremely high. Analysis of the LSM prepared using IOE method revealed that existing landslide areas fell into classes of of 0.17%—extremely low, 1.32%—low, 8.71%—moderate, 24.69%—high and 65.11%—extremely high. In the LSM prepared using the combined method, landslide areas were found to be composed of 0%—extremely low, 0.65%—low, 4.42%—moderate, 18.09%—high and 76.84%—extremely high (Table 7).

Table 6. IOE values for causative factors.

Factor	Class	No. of Pixels in Domain	Percentage of Domain	No. of Landslide	Percentage of Landslide	Pij	(Pij)	Hj	Hj max	Ij	Wj
SLOPE (Deg)	0–10	1,527,794	60.43	14,109	32.72	0.54	0.08	2.23	2.32	0.04	0.05
	10–20	678,851	26.85	19,454	45.12	1.68	0.24				
	20–30	266,839	10.55	7966	18.47	1.75	0.25				
	30–40	49,548	1.96	1491	3.46	1.76	0.26				
	>40	5163	0.20	100	0.23	1.14	0.17				
Aspect	Flat	29,326	1.16	0	0.00	0.00	0.00	2.87	3.17	0.09	0.09
	N	312,627	12.37	3910	9.07	0.73	0.09				
	NE	259,456	10.26	2174	5.04	0.49	0.06				
	E	247,899	9.81	5175	12.00	1.22	0.15				
	SE	299,619	11.85	7315	16.96	1.43	0.18				
	S	338,804	13.40	10,140	23.52	1.75	0.22				
	SW	330,225	13.06	5856	13.58	1.04	0.13				
	W	343,688	13.59	4858	11.27	0.83	0.10				
	NW	366,551	14.50	3692	8.56	0.59	0.07				
SPI	Low	434,163	17.17	4457	10.34	0.60	0.15	1.78	2.00	0.11	0.11
	Moderate	667,197	26.39	3997	9.27	0.35	0.09				
	High	1,145,730	45.32	26,856	62.28	1.37	0.35				
	Ex. high	281,105	11.12	7810	18.11	1.63	0.41				
Distance from stream (m)	0–100	628,808	24.87	8536	19.80	0.80	0.16	2.31	2.32	0.00	0.00
	100–200	536,113	21.21	8353	19.37	0.91	0.18				
	200–300	450,044	17.80	7591	17.60	0.99	0.20				
	300–400	377,276	14.92	6863	15.92	1.07	0.21				
	>400	535,954	21.20	11,777	27.31	1.29	0.26				
Density of discontinuity	Low	803,727	31.79	2925	6.78	0.21	0.05	1.75	2.00	0.13	0.15
	Moderate	766,508	30.32	14,173	32.87	1.08	0.23				
	High	720,240	28.49	18,236	42.29	1.48	0.32				
	Ex. high	237,720	9.40	7786	18.06	1.92	0.41				
Curvature	Convex	367,398	14.53	9300	21.57	1.48	0.42	1.55	1.59	0.03	0.03
	Plain	1,773,818	70.16	25,822	59.88	0.85	0.24				
	Concave	386,979	15.31	7998	18.55	1.21	0.34				
Lithology	Qalv	750,212	29.71	213	0.49	0.02	0.00	2.19	3.32	0.34	0.23
	Vlr	362,782	14.37	15,952	36.99	2.57	0.38				
	Lms	201,654	7.99	4715	10.93	1.37	0.20				
	Qsv	7848	0.31	0	0.00	0.00	0.00				
	SnSh	688,762	27.28	11,822	27.42	1.00	0.15				
	Vsd	9260	0.37	0	0.00	0.00	0.00				
	Plc	30,337	1.20	0	0.00	0.00	0.00				
	Dcr	429,522	17.01	10,267	23.81	1.40	0.21				
	Srp	21,359	0.85	120	0.28	0.33	0.05				
	Kfm	22,983	0.91	0	0.00	0.00	0.00				
Elevation (m)	0–50	607,148	24.02	458	1.06	0.04	0.00	3.10	3.17	0.02	0.03
	50–100	161,965	6.41	4105	9.52	1.49	0.14				
	100–150	219,961	8.70	5473	12.69	1.46	0.14				
	150–200	175,781	6.95	4764	11.05	1.59	0.15				
	200–250	209,613	8.29	3342	7.75	0.93	0.09				
	250–300	170,361	6.74	4115	9.54	1.42	0.13				
	300–350	154,400	6.11	3352	7.77	1.27	0.12				
	350–400	125,978	4.98	2701	6.26	1.26	0.12				
	>400	702,988	27.81	14,810	34.35	1.24	0.12				
Land use	Settlement	362,269	14.33	4607	10.68	0.75	0.19	1.93	2.00	0.04	0.03
	Field	731,306	28.93	12,645	29.33	1.01	0.26				
	Dry land	690,159	27.30	17,266	40.04	1.47	0.38				
	Forest	742,845	29.38	8602	19.95	0.68	0.17				

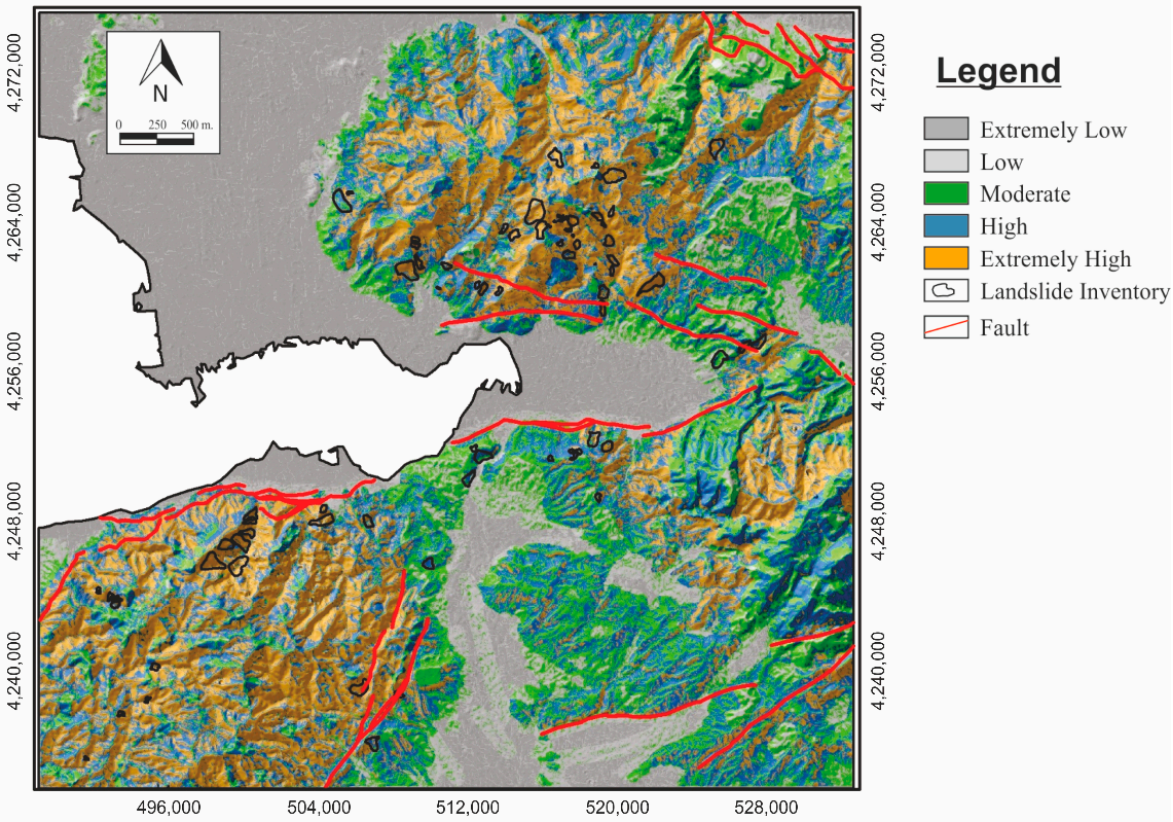

Figure 10. Landslide susceptibility map prepared with IOE method.

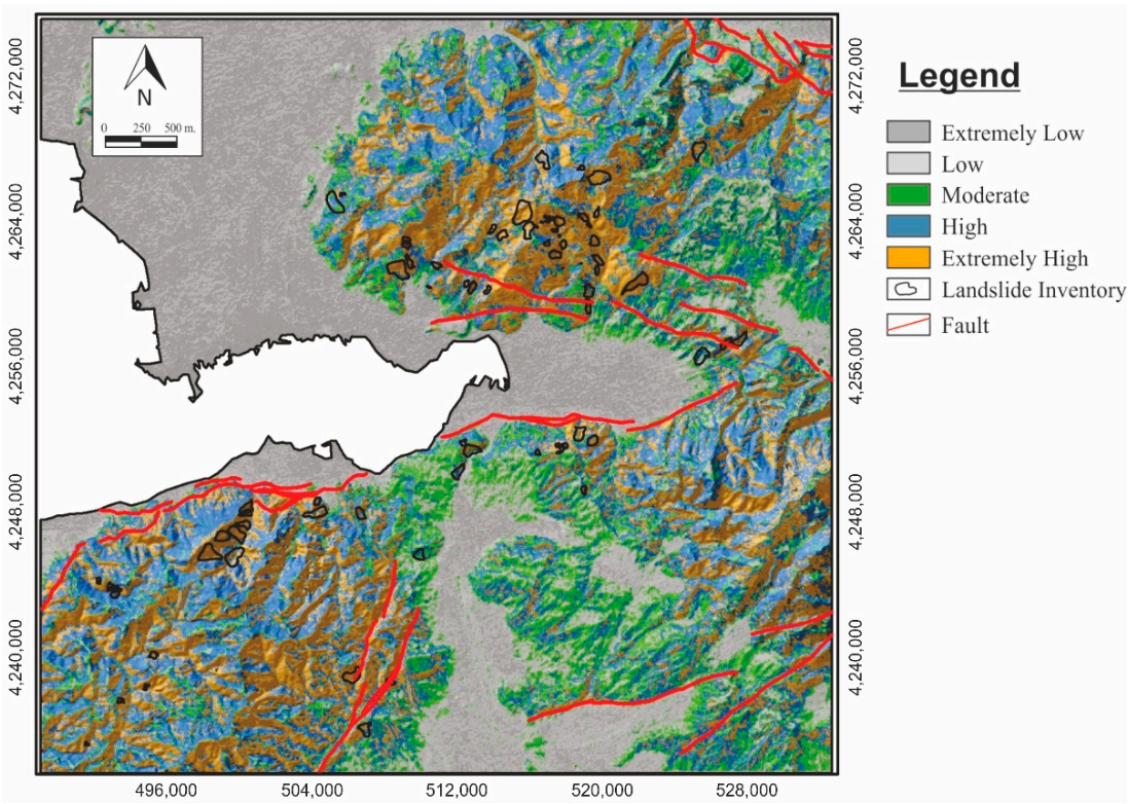

Figure 11. Landslide susceptibility map prepared with the combined method.

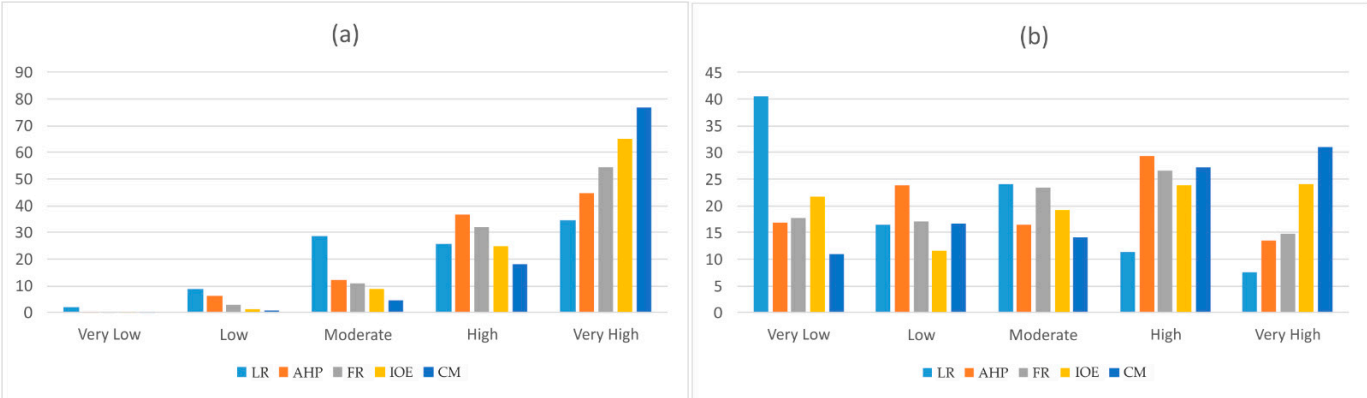

Figure 12. (**a**) Landslide susceptibility distribution of five classes in landslide inventory, (**b**) Landslide susceptibility distribution of five classes for whole study area.

Table 7. Percentages of susceptibility classes according to the method used.

	Extremely Low	Low	Moderate	High	Extremely High
LR	2.07%	8.84%	28.82%	25.57%	34.7%
AHP	0.19%	6.27%	12.01%	36.7%	44.84%
FR	0.18%	2.72%	10.93%	31.88%	54.29%
IOE	0.17%	1.32%	8.71%	24.69%	65.11%
CM	0%	0.65%	4.42%	18.09%	76.84%

4.2. Evaluation of Model Performance

As can be seen from the table of the Pearson's correlation of coefficient matrix given below, all the correlation coefficients between different independent variables were less than abs (0.80). In essence, the parameters used in the construction of the models were carefully selected for susceptibility analysis, and these parameters can be considered not to be physically related with each other. The Pearson's correlation coefficient matrix proves that the independent variables did not have a multi-collinearity problem (Table 8).

Table 8. Pearson's correlation of coefficient matrix.

Parameter	1	2	3	4	5	6	7	8	9
(1) Slope aspect	1								
(2) Density of discontinuity	−0.16	1							
(3) Lithology	−0.40	0.65	1						
(4) Slope	−0.55	0.66	0.47	1					
(5) SPI	0.46	0.59	−0.03	−0.03	1				
(6) Slope curvature	0.68	0.05	−0.24	0.04	−0.04	1			
(7) Elevation	−0.48	0.45	0.15	0.65	−0.27	−0.61	1		
(8) Land use	−0.31	−0.10	0.38	0.48	−0.68	0.47	0.30	1	
(9) Distance from stream	−0.43	−0.48	0.41	−0.41	−0.67	−0.69	0.23	0.18	1

The basic statistics of the outputs obtained by use of five methods are given in Table 9. It can be seen that the mean of CM and IOE are close to each other. The variances of remaining three methods are close to each other. Negative kurtosis coefficients indicate that the distribution has a lighter tail than a normal distribution. The negative skewness coefficients prove that similar behavior is observed for all model outputs, skewed to the left.

Table 9. Basic statistics of outputs covering whole study area.

	CM	*LR*	*AHP*	*FR*	*IOE*
Mean	3.2573	2.3028	3.0243	3.0641	3.2090
Standard Error	0.0174	0.0164	0.0164	0.0165	0.0182
Median	4	2	3	3	3
Mode	4	1	4	4	5
Standard Deviation	1.3845	1.3037	1.3021	1.3149	1.4452
Sample Variance	1.9168	1.6998	1.6956	1.7290	2.0886
Kurtosis	−1.23344	−0.864065733	−1.207652717	−1.106893346	−1.25068
Skewness	−0.26904	0.559431068	−0.093076809	−0.161480185	−0.28333
Range	4	4	4	4	4
Minimum	1	1	1	1	1
Maximum	5	5	5	5	5
Sum	20.476	14.476	19.011	19.261	20.172
Count	6286	6286	6286	6286	6286

5,4,3,2. and 1 in LSM correspond to susceptibilities of extremely high, high, moderate, low and extremely low.

In order to question if the means of five models are significantly different from each other, t-tests were performed. A null hypothesis was identified: the means of two outputs were the same. The results obtained from the CM were compared with the outputs of the four remaining models. The t-test values were 39.79, 9.72, 8.02 and 1.91 for the four pairs, CM/LR, CM/AHP, CM/FR and CM/IOE, respectively. The corresponding critical t-values were in the vicinity of 1.64. The null hypothesis was rejected in these four analyses. Moreover, Friedman tests were employed to determine whether there was a statistically significant difference between the means of the outputs. For our extremely large database, the p-values were extremely low, and the results were not sufficiently meaningful to present here.

The AUC (Area Under the ROC curve) is an important parameter (Chen et al. [122]; Lv et al. [123]) which gives valuable information about the accuracy of any model. For a perfect application, this parameter should be equal to 1.0. The threshold for random chance is 1.5. Following the ROC curves obtained by the various methods reveals that CM outperformed the other four methods (Figure 13).

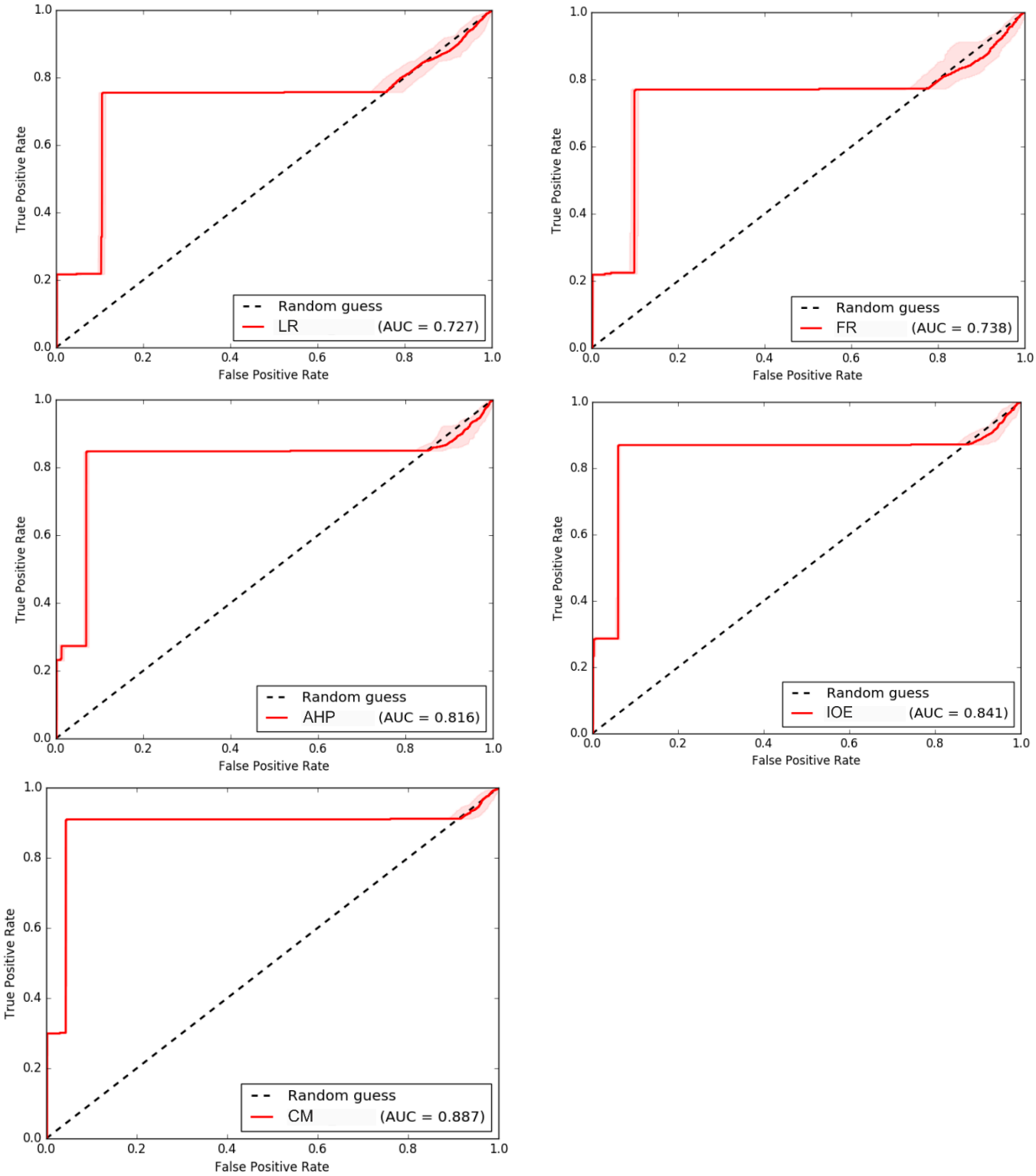

Figure 13. ROC curves of the LR, FR, AHP, IOE and CM methods.

5. Conclusions

A landslide inventory map was compiled using previously mapped literature from GDMRE [84] and Avsar [83]. With the help of landsat images and aerial photos, this map was then updated and a final landslide inventory map was prepared. When the final landslide inventory map was analyzed, it was determined that 0.86% of the total area is covered by existing landslide areas.

The geo-environmental factors of slope angle, slope aspect, lithology, slope curvature, elevation, density of discontinuity, stream power index (SPI), land use and distance to stream were used to determine landslide susceptibility. The data obtained was standardized in values of 0–1 using a fuzzy logic algorithm.

In the landslide susceptibility analysis studies conducted so far, generally one or a few LSMs are produced and the results of these maps are compared. It is evident that maps composed using different methods will produce different results. This study aims to minimise the negative effects of the errors that might arise from the shortcomings of each method for creating LSMs by making use of these differences and integrating maps prepared using different methods. In this study, LSMs were first prepared using the LR, AHP, FR and IOE methods, as the methods most commonly used recently, and then the final LSM was prepared using the combined method.

For determining success rates of the different methods used in this study, conformities between LSMs and the landslide inventory map were compared. Total areas of high and extremely high landslide susceptibility were compared with existing landslide localities. Success rates were calculated using these results. Success rates of 60.27%, 81.53%, 86.17% and 89.80% corresponded to the LR, AHP, FR and IOE LSMs, respectively. The best method—the combined method, which is combination of the LR, AHP, FR and IOE methods—had a success rate of 94.93%.

This study offers a preliminary guide for local authorities, engineers working in practice and academics working in this field. The results are promising, and were verified based on real-life phenomena. The results can constitute the basis of risk-based maps in the region.

The approach certainly has several limitations. Cartographic scale datasets were used for modelling; this causes unreliability in spatial analysis, which necessitates detailed field investigation. For instance, the geological data were obtained from the lithological map with a spatial resolution of approximately 25 × 25 m, but the GDEM used has a spatial resolution of 30 m. In should be noted that this is a preliminary approach for landslide susceptibility assessment.

Author Contributions: Conceptualization, C.K.; methodology, C.K. and H.K.; software, C.K. and H.K.; validation, C.K. and H.K.; formal analysis, H.K.; investigation, C.K. and H.K.; resources, C.K.; data curation, C.K. and H.K.; writing—original draft preparation, C.K. and H.K.; writing—review and editing, C.K. and H.K.; visualization, C.K. and H.K.; supervision, C.K.; project administration, C.K.; funding acquisition, C.K. and H.K. All authors have read and agreed to the published version of the manuscript.

Funding: This research received no external funding.

Institutional Review Board Statement: Not applicable.

Informed Consent Statement: Not applicable.

Data Availability Statement: Data available on request due to privacy restrictions. The data presented in this study are available on request from the corresponding author.

Acknowledgments: The authors are grateful to Alper SEZER for his support in statistical analyses and Enes Kalhan for his support in use of ArcMap software. Critical reviews by four anonymous reviewers in an earlier version of this manuscript are gratefully acknowledged. The authors also appreciate the contribution of Şeyda KINCAL for her support in language editing.

Conflicts of Interest: The authors declare no conflict of interest.

References

1. USGS. 2021. Available online: https://www.usgs.gov/faqs/what-landslide-and-what-causes-one (accessed on 3 May 2021).
2. Raghuvanshi, T.K. Plane failure in rock slopes—A review on stability analysis techniques. *J. King Saud Univ.–Sci.* **2019**, *31*, 101–109. [CrossRef]
3. Samanta, S.K.; Majumdar, R.K.; Chowdhury, S. Modes of slope failure in layered rocks of landslide zones: Insight from finite element modelling. *Indian J. Geosci.* **2015**, *69*, 117–130.

4. Hack, R.; Alkema, D.; Kruse, G.A.M.; Leenders, N.; Luzi, L. Influence of earthquakes on the stability of slopes. *Eng. Geol.* **2007**, *91*, 4–15. [CrossRef]
5. Park, S.; Kim, W.; Lee, J.; Baek, Y. Case Study on Slope Stability Changes Caused by Earthquakes—Focusing on Gyeongju 5.8 ML EQ. *Sustainability* **2018**, *10*, 3441. [CrossRef]
6. Rupke, J.M.; Huisman, M.; Kruse, H.M.G. Stability of man-made slopes. *Eng. Geol.* **2007**, *91*, 16–24. [CrossRef]
7. Kolapo, P.; Oniyide, G.O.; Said, K.O.; Lawal, A.I.; Onifade, M.; Munemo, P. An Overview of Slope Failure in Mining Operations. *Mining* **2022**, *2*, 350–384. [CrossRef]
8. Çevik, E.; Topal, T. GIS-based landslide susceptibility mapping for a problematic segment of the natural gas pipeline, Hendek (Turkey). *Environ. Geol.* **2003**, *44*, 949–962. [CrossRef]
9. Lee, S. Application of logistic regression model and its validation for landslide susceptibility mapping using GIS and remote sensing data. *Int. J. Remote Sens.* **2005**, *26*, 1477–1491. [CrossRef]
10. Yalcin, A.; Reis, S.; Aydinoglu, A.C.; Yomralioglu, T. A GIS-based comparative study of frequency ratio, analytical hierarchy process, bivariate statistics and logistics regression methods for landslide susceptibility mapping in Trabzon, NE Turkey. *CATENA* **2011**, *85*, 274–287. [CrossRef]
11. Pourghasemi, H.R.; Pradhan, B.; Gokceoglu, C. Application of fuzzy logic and analytical hierarchy process (AHP) to landslide susceptibility mapping at Haraz watershed, Iran. *Nat. Hazards* **2012**, *63*, 965–996. [CrossRef]
12. Shahabi, H.; Khezri, S.; Bin Ahmad, B.; Hashim, M. Landslide susceptibility mapping at central Zab basin, Iran: A comparison between analytical hierarchy process, frequency ratio and logistic regression models. *CATENA* **2014**, *115*, 55–70. [CrossRef]
13. Pham, B.T.; Bui, D.T.; Pourghasemi, H.R.; Indra, P.; Dholakia, M.B. Landslide susceptibility assesssment in the Uttarakhand area (India) using GIS: A comparison study of prediction capability of naïve bayes, multilayer perceptron neural networks, and functional trees methods. *Theor. Appl. Climatol.* **2017**, *128*, 255–273. [CrossRef]
14. Abedini, N.; Tulabi, S. Assessing LNRF, FR, and AHP models in landslide susceptibility mapping index: A comparative study of Nojian watershed in Lorestan province, Iran. *Enviromental Earth Sci.* **2018**, *77*, 405. [CrossRef]
15. Du, G.; Zhang, Y.; Yang, Z.; Guo, C.; Yao, X.; Sun, D. Landslide susceptibility mapping in the region of eastern Himalayan syntaxis, Tibetan Plateau, China: A comparison between analytical hierarchy process information value and logistic regression-information value methods. *Bull. Eng. Geol. Environ.* **2018**, *78*, 4201–4215. [CrossRef]
16. Reichenbach, P.; Rossi, M.; Malamud, B.D.; Mihir, M.; Guzzetti, F. A review of statistically-based landslide susceptibility models. *Earth-Sci. Rev.* **2018**, *180*, 60–91. [CrossRef]
17. Talaei, R.A. Combined Model for Landslide Susceptibility, Hazard and Risk Assessment. *AUT J. Civ. Eng.* **2018**, *2*, 11–28.
18. Carabella, C.; Miccadei, E.; Paglia, G.; Sciarra, N. Post-Wildfire Landslide Hazard Assessment: The Case of the 2017 Montagna Del Morrone Fire (Central Apennines, Italy). *Geosciences* **2019**, *9*, 175. [CrossRef]
19. Demir, G. GIS-based landslide susceptibility mapping for a part of the North Anatolian Fault Zone between Resadiye and Koyulhisar (Turkey). *CATENA* **2019**, *183*, 104211. [CrossRef]
20. Konovalov, A.; Gensiorovskiy, Y.; Lobkina, V.; Muzychenko, A.; Stepnova, Y.; Muzychenko, L.; Stepnov, A.; Mikhalyov, M. Earthquake-Induced Landslide Risk Assessment: An Example from Sakhalin Island, Russia. *Geosciences* **2019**, *9*, 305. [CrossRef]
21. Saha, A.; Mandal, S.; Saha, S. Geo-spatial approach-based landslide susceptibility mapping using analytical hierarchical process, frequency ratio, logistic regression and their ensemble methods. *SN Appl. Sci.* **2020**, *2*, 1647. [CrossRef]
22. Sun, D.; Xu, J.; Wen, H.; Wang, D. Assessment of landslide susceptibility mapping based on Bayesian hyperparameter optimization: A comparison between logistic regression and random forest. *Eng. Geol.* **2021**, *281*, 105972. [CrossRef]
23. Wang, Y.; Frang, Z.; Hong, H.; Costache, R.; Tang, X. Flood susceptibility mapping by integrating frequency ratio and index of entropy with multilayer perceptron and classification and regression tree. *J. Environ. Manag.* **2021**, *289*, 112449. [CrossRef] [PubMed]
24. Carabella, C.; Cinosi, J.; Piattelli, V.; Burrato, P.; Miccadei, E. Earthquake-induced landslides susceptibility evaluation: A case study from the Abruzzo region (Central Italy). *CATENA* **2022**, *208*, 105729. [CrossRef]
25. Melese, T.; Belay, T.; Andemo, A. Application of analytical hierarchal process, frequency ratio, and Shannon entropy approaches for landslide susceptibility mapping using geospatial technology: The case of Dejen district, Ethiopia. *Arab. J. Geosci.* **2022**, *15*, 424. [CrossRef]
26. Chen, W.; Chai, H.; Sun, X.; Wang, Q.; Ding, X.; Hong, H. A GIS-based comparative study of frequency ratio, statistical index and weights-of-evidence models in landslide susceptibility mapping. *Arab. J. Geosci.* **2016**, *9*, 204. [CrossRef]
27. Lee, S.; Min, K. Statistical analysis of landslide susceptibility at Yongin, Korea. *Environ. Geol.* **2001**, *40*, 1095–1113. [CrossRef]
28. Suzen, M.L.; Doyuran, V. A comparison of the GIS based landslide susceptibility assessment methods: Multivariate versus bivariate. *Environ. Geol.* **2004**, *45*, 665–679. [CrossRef]
29. Lee, S.; Ryu, J.H.; Won, J.S.; Park, H.J. Determination and application of the weights for landslide susceptibility mapping using an artificial neural network. *Eng. Geol.* **2004**, *71*, 289–302. [CrossRef]
30. Yılmaz, I. Landslide susceptibility mapping using frequency ratio, logistic regression, artificial neural network sand their comparison: A case study from Kat landslides (Tokat -Turkey). *Comput. Geosci.* **2009**, *7*, 1125–1138. [CrossRef]
31. Suzen, M.L. Data Driven Landslide Hazard Assessment Using Geographical Information System and Remote Sensing. Ph.D. Thesis, Middle East Technical University, Ankara, Turkey, 2002.

32. Hong, H.; Pourghasemi, H.R.; Pourtaghi, Z.S. Landslide susceptibility assessment in Lianhua County (China): A comparison between a random forest data mining technique and bivariate and multivariate statistical models. *Geomorphology* **2016**, *259*, 105–118. [CrossRef]
33. Degirmenci, I. Entropy Measurement and Maximum Entropy Principle. Master's Thesis, Hacettepe University, Ankara, Turkey, 2011.
34. Zadeh, L.A. Shadows of fuzzy sets. *Probl. Peredachi Inf.* **1965**, *2*, 37–44.
35. Bathrellos, G.D.; Skilodimou, H.D.; Chousianitis, K.; Youssef, A.M.; Pradhan, B. Suitability estimation for urban development using multi-hazard assessment map. *Sci Total Environ.* **2017**, *575*, 119–134. [CrossRef] [PubMed]
36. Rahman, M.S.; Ahmed, B.; Di, L. Landslide initiation and runout susceptibility modeling in the context of hill cutting and rapid urbanization: A combined approach of weights of evidence and spatial multi-criteria. *J. Mt. Sci.* **2017**, *14*, 1919–1937. [CrossRef]
37. Achour, Y.; Boumezbeur, A.; Hadji, R.; Chouabbi, A.; Cavaleiro, V.; Bendaoud, E.A. Landslide susceptibility mapping using analytic hierarchy process and information value methods along a highway road section in Constantine, Algeria. *Arab. J. Geosci.* **2017**, *10*, 194. [CrossRef]
38. Sharma, S.; Kumar Mahajan, A. Comparative evaluation of GIS-based landslide susceptibility mapping using statistical and heuristic approach for Dharamshala region of Kangra Valley, India. *Geoenviron. Disasters* **2018**, *5*, 4. [CrossRef]
39. Ali, S.; Biermanns, P.; Haider, R.; Reicherter, K. Landslide susceptibility mapping by using GIS along the China–Pakistan economic corridor (Karakoram Highway), Pakistan. *Nat. Hazards Earth Syst. Sci. Discuss.* **2018**, *19*, 999–1022. [CrossRef]
40. Akgun, A.; Turk, N. Landslide susceptibility mapping for Ayvalik (Western Turkey) and its vicinity by multicriteria decision analysis. *Environ. Earth Sci.* **2010**, *61*, 595–611. [CrossRef]
41. Saaty, T.L.; Vargas, L. The Analytic Network Process. In *Decision Making with the Analytic Network Process*; Springer: Boston, MA, USA, 2006; pp. 1–26. [CrossRef]
42. Pradhan, B. A comparative study on the predictive ability of the decision tree, support vector machine and neuro-fuzzy models in landslide susceptibility mapping using GIS. *Comput Geosci.* **2013**, *51*, 350–365. [CrossRef]
43. Shirzadi, A.; Bui, D.T.; Pham, B.T.; Solaimani, K. Shallow landslide susceptibility assessment using a novel hybrid intelligence approach. *Environ. Earth Sci.* **2017**, *76*, 60. [CrossRef]
44. Chen, W.; Li, X.; Wang, Y.; Chen, G.; Liu, S. Forested landslide detection using LiDAR data and the random forest algorithm: A case study of the Three Gorges, China. *Remote Sens. Environ.* **2014**, *152*, 291–301. [CrossRef]
45. Paudel, U.; Oguchi, T.; Hayakawa, Y. Multi-resolution landslide susceptibility analysis using a DEM and random forest. *Int. J. Geosci.* **2016**, *07*, 726–743. [CrossRef]
46. Zhang, K.; Wu, X.; Niu, R.; Yang, K.; Zhao, L. The assessment of landslide susceptibility mapping using random forest and decision tree methods in the three Gorges reservoir area, China. *Environ. Earth Sci.* **2017**, *76*, 405. [CrossRef]
47. Kim, J.; Lee, S.; Jung, H.; Lee, S. Landslide susceptibility mapping using random forest and boosted tree models in Pyeong-Chang, Korea. *J. Geocarto Int.* **2018**, *33*, 1000–1015. [CrossRef]
48. Taalab, K.; Cheng, T.; Zhang, Y. Mapping landslide susceptibility and types using Random Forest. *Big Earth Data* **2018**, *2*, 159–178. [CrossRef]
49. Iovine, G.; Greco, R.; Gariano, S.L.; Pellegrino, A.D.; Terranova, O.G. Shallow-landslide susceptibility in the Costa Viola mountain ridge (Southern Calabria, Italy) with considerations on the role of causal factors. *Nat. Hazards* **2014**, *73*, 111–136. [CrossRef]
50. Karimi Sangchini, E.K.; Emami, S.N.; Tahmasebipour, N.; Pourghasemi, H.R.; Naghibi, S.A.; Wu, Z.; Wu, Y.; Yang, Y.; Chen, F.; Zhang, N.; et al. A comparative study on the landslide susceptibility mapping using logistic regression and statistical index models. *Arab. J. Geosci.* **2017**, *10*, 187.
51. Polykretis, C.; Faka, A.; Chalkias, C. Exploring the Impact of Analysis Scale on Landslide Susceptibility Modeling: Empirical Assessment in Northern Peloponnese, Greece. *Geosciences* **2018**, *8*, 261. [CrossRef]
52. Atkinson, P.M.; Massari, R. Generalized linear modelling of landslide susceptibility in the Central Apennines, Italy. *Comput. Geosci.* **1998**, *24*, 373–385. [CrossRef]
53. Dai, F.C.; Lee, C.F. Landslide characteristics and slope instability modeling using GIS, Lantau Island, Hong Kong. *Geomorphology* **2002**, *42*, 213–228. [CrossRef]
54. Akgun, A.; Bulut, F. GIS-based landslide susceptibility for Arsin-Yomra (Trabzon, North Turkey) region. *Environ. Geol.* **2007**, *51*, 1377–1387. [CrossRef]
55. Akgun, A. A comparison of landslide susceptibility maps produced by logistic regression, multi-criteria decision, and likelihood ratio methods: A case study at İzmir, Turkey. *Landslides* **2012**, *9*, 93–106. [CrossRef]
56. Akgun, A.; Kıncal, C.; Pradhan, B. Application of remote sensing data and GIS for landslide risk assessment as an environmental threat to Izmir city (west Turkey). *Environ. Monit. Assess.* **2012**, *184*, 5453–5470. [CrossRef] [PubMed]
57. Kıncal, C.; Akgun, A.; Koca, M.Y. Landslide susceptibility assessment in the Izmir (West Anatolia, Turkey) city center and its near vicinity by the logistic regression method. *Environ. Earth Sci.* **2009**, *59*, 745–756. [CrossRef]
58. Pradhan, B.; Lee, S.; Buchroithner, M.F. Use of geospatial data for the development of fuzzy algebraic operators to landslide hazard mapping: A case study in Malaysia. *Appl. Geomat.* **2009**, *1*, 3–15. [CrossRef]
59. Gorsevski, P.V.; Brown, M.K.; Panter, K.; Onasch, C.M. Landslide detection and susceptibility mapping using LiDAR and an artificial neural network approach: A case study in the Cuyahoga Valley National Park, Ohio. *Landslides* **2016**, *13*, 467–484. [CrossRef]

60. Crozier, M.J.; Glade, T. *Landslide Hazard and Risk: Issues, Concepts and Approach*; Glade, T., Anderson, M.G., Crozier, M.J., Eds.; Landslide Risk Assessment; John Wiley: New York, NY, USA, 2005; pp. 1–40. [CrossRef]
61. Yüksel, N. Usage of Statistical Methods and Artificial Neural Networks in Geographical Information Systems Based Landslide Susceptibility Mapping: Kumluca-Ulus (Bartın-Türkiye) Region. Ph.D. Thesis, Hacettepe University, Institute of Natural and Applied Sciences, Ankara, Turkey, 2007. (In Turkish)
62. Tantuğ, A.C.; ve Türkmenoğlu, C. Türkçe Metinlerde Duygu Analizi. Master's Thesis, İstanbul Teknik Üniversitesi, İstanbul, Turkey, 2015.
63. Çelik, O. A Research on Machine Learning Methods and Its Applications. *J. Educ. Technol. Online Learn.* **2018**, *1*, 25–40. [CrossRef]
64. Do, H.M.; Kun, L.Y.; Zi, Z.G. A comparative study on the integrative ability of the analytical hierarchy process, weights of evidence and logistic regression methods with the Flow-R model for landslide susceptibility assessment. *Geomat. Nat. Hazards Risk* **2020**, *11*, 2449–2485. [CrossRef]
65. Fang, Z.; Wang, Y.; Peng, L.; Hong, H. A comparative study of heterogeneous ensemble-learning techniques for landslide susceptibility mapping. *Int. J. Geogr. Inf. Sci.* **2020**, *35*, 321–347. [CrossRef]
66. Arabameri, A.; Pradhan, B.; Rezaei, K.; Lee, S.; Sohrabi, M. An ensemble model for landslide susceptibility mapping in a forested area. *Geocarto Int.* **2020**, *35*, 1680–1705. [CrossRef]
67. Iban, C.M.; Sekertekin, A. Machine learning based wildfire susceptibility mapping using remotely sensed fire data and GIS: A case study of Adana and Mersin provinces, Turkey. *Ecol. Inform.* **2022**, *69*, 101647. [CrossRef]
68. Saleh, A.; Yuzir, A.; Sabtu, N.; Abujayyab, S.K.M.; Bunmi, M.R.; Pham, Q.B. Flash flood susceptibility mapping in urban area using genetic algorithm and ensemble method. *Geocarto Int.* **2022**, 1–30. [CrossRef]
69. Arabameri, A.; Pal, S.C.; Costache, R.; Saha, A.; Rezaie, F.; Danesh, A.S.; Pradhan, B.; Lee, S.; Hoang, N.D. Prediction of gully erosion susceptibility mapping using novel ensemble machine learning algorithms. *Geomat. Nat. Hazards Risk* **2021**, *1*, 469–498. [CrossRef]
70. Izmir Governorship. Available online: http://www.izmir.gov.tr/istatistiklerle-izmir (accessed on 8 September 2020).
71. MGM, Turkish State Meteorological Service. Available online: https://www.mgm.gov.tr/veridegerlendirme/il-ve-ilceler-istatistik.aspx?k=A&m=IZMIR (accessed on 8 September 2020).
72. Kıncal, C. Engineering Geological Evaluation of Geological Units Outcrop in and around the Izmir City Centre with the Help of Geographical Information Systems and Remote Sensing Techniques. Ph.D. Thesis, The Graduate School of Natural and Applied Sciences, Dokuz Eylul University, Izmir, Turkey, 2005; p. 342. (In Turkish)
73. Erdogan, B. Tectonic Relations between İzmir-Ankara Zone and Karaburun Belt. *Bull. Turk. Assoc. Pet. Geol.* **1990**, *2*, 20.
74. Ersoy, E.Y.; Dindi, F.; Karaoğlu, Ö.; Helvacı, C. Geochemical and petrographic features of the Miocene volcanism around Soma basin, western Anatolia, Turkey. *Earth Sci.* **2012**, *33*, 59–80.
75. GDMRE. *Geological Map of Turkey 2000. 1.25000-Scaled Izmir Sheet*; General Directorate of Mineral Research and Exploration of Turkey: Ankara, Turkey, 2000.
76. Genc, S.C.; Altunkaynak, S.; Karacik, Z.; Yazman, M.; Yılmaz, Y. The Çubukludağ graben, South of Izmir: Tectonic significance in the Neogene geological evolution of the Western Anatolia. *Geodin. Acta* **2001**, *14*, 1–12.
77. Akartuna, M. On the geology of Izmir, Torbalı, Seferhisar, Urla districts. *MTA Bull.* **1962**, *59*, 1–19.
78. Chung, C.-J.F.; Fabbri, A.G. Probabilistic Prediction Models for Landslide Hazard Mapping. *Photogramm. Eng. Remote Sens.* **1999**, *65*, 1389–1399.
79. Choi, J.; Oh, H.J.; Lee, H.J.; Lee, C.; Lee, S. Combining landslide susceptibility maps obtained from frequency ratio, logistic regression, and artificial neural network models using aster images and GIS. *Eng. Geol.* **2011**, *124*, 12–23. [CrossRef]
80. Umar, Z.; Pradhan, B.; Ahmad, A.; Jebur, M.N.; Tehrany, M.S. Earthquake induced landslide susceptibility mapping using an integrated ensemble frequency ratio and logistic regression models in West Sumatera Province, Indonesia. *CATENA* **2014**, *118*, 124–135. [CrossRef]
81. Avsar, M. General Assessment of Landslides in Izmir Metropolitan Area. Master's Thesis, The Graduate School of Natural and Applied Sciences, Dokuz Eylul University, Izmir, Turkey, 1997.
82. GDMRE. GeoScience Map Viewer and Drawing Editor. General Directorate of Mineral Research and Exploration of Turkey. Available online: http://yerbilimleri.mta.gov.tr/anasayfa.aspx (accessed on 9 March 2020).
83. Carrara, A.; Guzzetti, F.; Cardinali, M.; Reichenbach, P. Use of GIS technology in the prediction and monitoring of landslide hazard. *Nat. Hazards* **1999**, *20*, 117–135. [CrossRef]
84. Guzzetti, F.; Carrara, A.; Cardinali, M.; Reichenbach, P. Landslide hazard evaluation: A review of current techniques and their application in a multi-scale study, Central Italy. *Geomorphology* **1999**, *31*, 181–216. [CrossRef]
85. Soeters, R.; Van Westen, C.J. Slope instability recognition, analysis and zonation. *Landslides Investig. Mitig.* **1996**, *247*, 129–177.
86. Djukem, W.D.L.; Braun, A.; Wouatong, A.S.L.; Guedjeo, C.; Dohmen, K.; Wotchoko, P.; Fernandes-Steeger, T.M.; Havenith, H.B. Effect of soil geomechanical properties and geo-environmental factors on landslide predisposition at mount oku, cameroon. *Int. J. Environ. Res. Public Health* **2020**, *17*, 6795. [CrossRef] [PubMed]
87. ASTER GDEM. Available online: http://earthexplorer.usgs.gov (accessed on 10 June 2020).
88. Google Earth Satellite Images. Available online: https://earth.google.com/web/ (accessed on 10 May 2021).
89. Cellek, S. Effect of the slope angle and its classification on landslides. *Himal. Geol.* **2022**, *43*, 85–95.

90. Galli, M.; Francesca, A.; Cardinali, M.; Guzzetti, F.; Reichenbach, P. Comparing landslide inventory maps. *Geomorphology* **2008**, *94*, 268–289. [CrossRef]
91. Lee, S.; Dan, N.T. Probabilistic landslide susceptibility mapping in the Lai Chau province of Vietnam: Focus on the relationship between tectonic fractures and landslides. *Environ. Geol.* **2005**, *48*, 778–787. [CrossRef]
92. Yalcin, A.; Bulut, F. Landslide susceptibility mapping using GIS and digital photogrammetric techniques: A case study from Ardeşen (NE-Turkey). *Nat. Hazards* **2007**, *41*, 201–226. [CrossRef]
93. Costanzo, D.; Rotigliano, E.; Irigaray, C.; Jiménez-Perálvarez, J.D.; Chacón, J. Factors selection in landslide susceptibility modelling on large scale following the gis matrix method: Application to the river Beiro basin (Spain). *Nat. Hazards Earth Syst. Sci.* **2012**, *12*, 327–340. [CrossRef]
94. Pradhan, B.; Lee, S. Landslide susceptibility assessment and factor effect analysis: Backpropagation artificial neural networks and their comparison with frequency ratio and bivariate logistic regression modelling. *Environ. Modeling Softw.* **2010**, *25*, 747–759. [CrossRef]
95. ArcMap. Software Manual 2020. Available online: https://arcmap.nersc.no/pdfs/User-Manual-ARCMAP-05-2020-English.pdf (accessed on 5 May 2020).
96. Ohlmacher, G.C. Plan curvature and landslide probability in regions dominated by earth flows and earth slides. *Eng. Geol.* **2007**, *91*, 117–134. [CrossRef]
97. Catani, F.; Lagomarsino, D.; Segoni, S.; Tofani, V. Landslide susceptibility estimation by random forests technique: Sensitivity and scaling issues. *Nat. Hazards Earth Syst. Sci.* **2013**, *13*, 2815–2831. [CrossRef]
98. Bastug, G. Preperation of Landslide Susceptibilty Map of Adrasan and Olimpos (Antalya) Regions. Master's Thesis, Hacettepe University, Ankara, Turkey, 2018.
99. Tetik Bicer, C. A Semi-Quantitative Evaluation of Landslide Risk Mapping. Ph.D. Thesis, Hacettepe University, Ankara, Turkey, 2017.
100. Zezere, J.L. Landslide susceptibility assessment considering landslide typology. A case study in the area north of Lisbon (Portugal). *Nat. Hazards Earth Syst. Sci.* **2002**, *2*, 73–82. [CrossRef]
101. Ayalew, L.; Yamagishi, H. The application of GIS-based logistic regression for susceptibility mapping in the Kakuda-Yahiko Mountains, Central Japan. *Geomorphology* **2005**, *65*, 15–31. [CrossRef]
102. Bai, S.B.; Wang, J.; Lü, G.N.; Zhou, P.G.; Hou, S.S.; Xu, S.N. GIS-based logistic regression for landslide susceptibility mapping of the Zhongxian segment in the Three Gorges area, China. *Geomorphology* **2010**, *115*, 23–31. [CrossRef]
103. Lee, S.; Pradhan, B. Landslide hazard mapping at Selangor, Malaysia using frequency ratio and logistic regression models. *Landslides* **2007**, *4*, 33–41. [CrossRef]
104. Idrisi. Software Manual 2020. Available online: https://clarklabs.org/wp-content/uploads/2020/05/Terrset-Manual.pdf (accessed on 5 May 2020).
105. Clark, W.A.V.; Hosking, P.L. Statistical methods for geographers. *Cah. Géographie Québec* **1986**, *31*, 91–92.
106. Saaty, T.L. *The Analytical Hierarchy Processes*; McGraw-Hill: New York, NY, USA, 1980.
107. Ayalew, L.; Hiromitsu, Y.; Norimitsu, U. Landslide susceptibility mapping using GIS-based weighted linear combination, the case in Tsugawa area of Agano River, Niigata Prefecture, Japan. *Landslides* **2004**, *1*, 73–81. [CrossRef]
108. Saaty, T.L.; Vargas, L.G. *Prediction, Projectionand Forecasting 2008*; Kluwer: New York, NY, USA, 1991.
109. Saaty, T.L. Ascaling method for priorities in hierarchical structure. *J. Math. Psychol.* **1977**, *15*, 34–39. [CrossRef]
110. Malczewski, J. *GIS and Multi-Criteria Decision Analysis*; John Wiley: New York, NY, USA, 1999.
111. Lee, S.; Thalib, J.A. Probabilistic landslide susceptibility and factor effect analysis. *Environ. Geol.* **2005**, *47*, 982–990. [CrossRef]
112. Yufeng, S.; Fengxiang, J. Landslide stability analysis based on generalized information entropy. In Proceedings of the 2009 International Conference on Environmental Science and Information Application Technology, Wuhan, China, 4–5 July 2009; pp. 83–85. [CrossRef]
113. Shannon, C.E. A Mathematical Theory of Communication. *Bull. Syst. Technol. J.* **1948**, *27*, 379–423. [CrossRef]
114. Li, X.; Wang, K.; Liu, L.; Xin, J. Application of the entropy weight and topsis method in safety evaluation of coal mines. *Procedia Eng.* **2011**, *26*, 2085–2091. [CrossRef]
115. Mon, D.L.; Cheng, C.H.; Lin, J.C. Evaluating weapon system using fuzzy analytic hierarchy process based on entropy weight. *Fuzzy Sets Syst.* **1994**, *62*, 127–134. [CrossRef]
116. Ren, L.C. Disaster entropy: Conception and application. *J. Nat. Disasters* **2000**, *9*, 26–31.
117. Yang, Z.; Qiao, J. Entropy-based hazard degree assessment for typical landslides in the Three Gorges Area in "Landslide Disaster Mitigation in Three Gorges Reservoir, China". *Environ. Sci. Eng.* **2009**, 519–529. [CrossRef]
118. Youssef, A.M.; Al-Kathery, M.; Pradhan, B. Landslide susceptibility mapping at Al-Hasher Area, Jizan (Saudi Arabia) using GIS-based frequency ratio and index of entropy models. *Geosci. J.* **2015**, *19*, 113–134. [CrossRef]
119. Yang, Z.; Qiao, J.; Zhang, X. Regional Landslide Zonation based on Entropy Method in Three Gorges Area, China. In Proceedings of the Seventh International Conference on Fuzzy Systems and Knowledge Discovery 2010, FSKD 2010, Yantai, China, 10–12 August 2010; pp. 1336–1339.
120. Bednarik, M.; Magulová, B.; Matys, M.; Marschalko, M. Landslide susceptibility assessment of the Kralovany–Liptovsky Mikuláš railway case study. *Phys. Chem. Earth Part A/B/C* **2010**, *35*, 162–171. [CrossRef]

121. Devkota, K.C.; Regmi, A.D.; Pourghasemi, H.R.; Yoshida, K.; Pradhan, B.; Ryu, I.C.; Althuwaynee, O.F. Landslide susceptibility mapping using certainty factor, index of entropy and logistic regression models in GIS and their comparison at Mugling-Narayanghat road section in Nepal Himalaya. *Nat. Hazards* **2013**, *65*, 135–165. [CrossRef]
122. Chen, T.; Zhu, L.; Niu, R.; Trinder, J.; Peng, L.; Lei, T. Mapping landslide susceptibility at the Three Gorges Reservoir, China, using gradient boosting decision tree, random forest and information value models. *J. Mt. Sci.* **2020**, *17*, 670–685. [CrossRef]
123. Lv, L.; Chen, T.; Dou, J.; Plaza, A. A hybrid ensemble-based deep-learning framework for landslide susceptibility mapping. *Int. J. Appl. Earth Obs. Geoinf.* **2022**, *108*, 102713. [CrossRef]